Journal Pre-proof

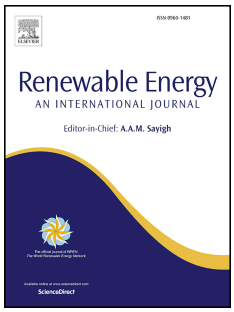

Phase change material-sand mixtures for distributed latent heat thermal energy storage: interaction and performance analysis

Silvia Barbi, Francesco Barbieri, Simona Marinelli, Bianca Rimini, Sebastiano Merchiori, Barbara Larwa, Michele Bottarelli, Monia Montorsi

PII: S0960-1481(21)00095-1

DOI: https://doi.org/10.1016/j.renene.2021.01.088

Reference: RENE 14827

To appear in: *Renewable Energy*

Received Date: 21 September 2020

Revised Date: 2 January 2021

Accepted Date: 17 January 2021

Please cite this article as: Barbi S, Barbieri F, Marinelli S, Rimini B, Merchiori S, Larwa B, Bottarelli M, Montorsi M, Phase change material-sand mixtures for distributed latent heat thermal energy storage: interaction and performance analysis, *Renewable Energy*, https://doi.org/10.1016/j.renene.2021.01.088.

CRediT author statement

Silvia Barbi: Investigation, Writing - Review & Editing. Francesco Barbieri: Investigation. Simona Marinelli: Writing - Original Draft. Bianca Rimini: Funding acquisition. Sebastiano Merchiori: Resources, Investigation, Methodology. Barbara Larwa: Resources. Michele Bottarelli: Conceptualization, Methodology. Monia Montorsi: Supervision.

Phase change material-sand mixtures for distributed latent heat thermal energy storage: interaction and performance analysis

Silvia Barbi[a*], Francesco Barbieri[b], Simona Marinelli[c], Bianca Rimini[b,c], Sebastiano Merchiori[e], Barbara Larwa[d], Michele Bottarelli[d,e], Monia Montorsi [b,c]

[a] *Interdepartmental Research Center for Industrial Research and Technology Transfer in the Field of Integrated Technologies for Sustainable Research, Efficient Energy Conversion, Energy Efficiency of Buildings, Lighting and Home Automation, University of Modena and Reggio Emilia, Via Amendola 2, 42122, Reggio Emilia, Italy.*

[b] *Interdepartmental center for applied research and services in advanced mechanics and motoring, INTERMECH-Mo.Re., University of Modena and Reggio Emilia, Via P. Vivarelli 10/1, 41125, Modena, Italy.*

[c] *Department of Science and Methods for Engineering, University of Modena and Reggio Emilia, Via Amendola 2, 42122, Reggio Emilia, Italy*

[d]*Department of Architecture, University of Ferrara, Via Quartieri 8, 44121, Ferrara, Italy*

[e] *TekneHub laboratory – University of Ferrara, Via Saragat 13, 44122, Ferrara, Italy*

**corresponding author: silvia.barbi@unimore.it tel.+39 059 2056281*

Phase change material-sand mixtures for distributed latent heat thermal energy storage: interaction and performance analysis

Silvia Barbi[a*], Francesco Barbieri[b], Simona Marinelli[c], Bianca Rimini[b,c], Sebastiano Merchiori[e], Barbara Larwa[d], Michele Bottarelli[d,e], Monia Montorsi [b,c]

[a] *Interdepartmental Research Center for Industrial Research and Technology Transfer in the Field of Integrated Technologies for Sustainable Research, Efficient Energy Conversion, Energy Efficiency of Buildings, Lighting and Home Automation, University of Modena and Reggio Emilia, Via Amendola 2, 42122, Reggio Emilia, Italy.*

[b] *Interdepartmental center for applied research and services in advanced mechanics and motoring, INTERMECH-Mo.Re., University of Modena and Reggio Emilia, Via P. Vivarelli 10/1, 41125, Modena, Italy.*

[c] *Department of Science and Methods for Engineering, University of Modena and Reggio Emilia, Via Amendola 2, 42122, Reggio Emilia, Italy*

[d]*Department of Architecture, University of Ferrara, Via Quartieri 8, 44121, Ferrara, Italy*

[e] *TekneHub laboratory – University of Ferrara, Via Saragat 13, 44122, Ferrara, Italy*

**corresponding author: silvia.barbi@unimore.it tel.+39 059 2056281*

Abstract

In this study two phase change materials (PCMs) mixed with sand were evaluated for distributed latent heat thermal energy storage (LHTES) coupled with a novel Flat-Panel ground heat exchanger (GHE) for shallow geothermal applications. *N*-Octadecane and a commercial paraffin-based PCM were mixed (30% v/v) separately with sand, which is commonly used as backfilling material for GHE. Both two mixtures underwent 16 thermal cycles and specimen's temperatures and their variation over time were analyzed to evaluate phase change stability and supercooling. Grain size laser diffraction and pore analysis were performed together with optical microscopy, environmental scanning electron microscopy coupled with X-Ray spectrometry (ESEM-EDS) and Fourier transform infrared spectroscopy (FTIR) analysis to evaluate PCMs-sand dynamic interaction over time and temperature. Results shown that sand addition halves *n*-Octadecane phase change time, although leading to a limited supercooling equal to 1 °C. Sand addition to commercial PCM leaded to a similar increasing in heat transfer, however in absence of supercooling phenomena. These performances were constant through 16 thermal cycles. Therefore, PCMs mixing in sand as mixture for GHEs backfilling material can be considered a strategy to enhance thermal storage of backfilling material, by increasing the underground thermal energy storage and then the exploitation carried out by shallow geothermal applications.

Keywords: Energy storage, backfilling sand, Flat-Panel ground heat exchanger, paraffin, *n*-Octadecane, building

Abbreviations	
S	Dry sand (type of sand: washed sand)
O	*n*-Octadecane
A28	A28 paraffin wax
OS	*n*-Octadecane-dry sand mix
AS	A28 paraffin wax-dry sand mix

1. Introduction

In 2015 the 30 % of global energy use and 28 % of CO_2 energy-related emissions were due to buildings technology [1]. Therefore, the European Energy Performance of Buildings Directive (EPBD) has established the need to decrease energy consumption and greenhouse gas emissions of buildings [2,3]. Despite efforts, such as improvements in building envelope performance and reduction of fossil fuel-based heating systems, buildings' energy efficiency is far to be environmentally sustainable [4]. In this context, the employment of more efficient technologies like Thermal Energy Storage (TES) coupled with Phase Change Materials (PCM) is a great opportunity. Although, sensible heat is currently the most employed type of TES, due to the fact that the thermal energy storage is reached through water temperature increase, latent heat TES (LHTES) allows the energy to be stored at a constant temperature and greater density [5–8]. This result is obtained through the choice of well-tailored phase change materials (PCMs), considering solid-liquid transition. Usually LHTES energy /volume ratio is between 5 and 14 times greater than sensible heat TES ratio, and this allows the size reduction of heating/cooling storage systems in buildings [8,9]. LHTES is realized through active or passive methods, depending on electric devices eventually employed [10]. Passive LHTES applications in buildings usually take in account PCMs addition and integration into building materials or elements such as concrete walls [11], insulating mortars [12], windows shutters [13]. Previous studied demonstrated that the incorporation of PCMs in construction elements potentially has positive environmental effects, even considering production, construction, and especially disposal burdens mainly linked to the non-biodegradability [14,15]. Among LHTES active applications, heat pumps coupling is the most interesting one in terms of high efficiency, as it is suitable for household heating and cooling, and environmental impact, reducing fossil fuel employment [16–19]. However, theirs performance depend widely on climatic and environmental conditions, therefore, several studies investigated heat pumps-LHTES integration with renewable energy systems (RES), e.g. photovoltaic modules and/or ground-based heat exchangers, which are also called ground coupled heat pumps (GCHP) [20–23]. Among GCHP, closed loop architectures, in which the heat working fluid circulates in a closed system developing in a borehole called Ground Heat Exchanger (GHE) and separated from the ground, are generally preferred. In fact, GHE doesn't depend on groundwater availability and quality, and doesn't suffer from critical issues like corrosive agents, scaling or bacterial contents [24]. Nevertheless, the depth of the borehole could arise some critical issues: greater depth (80-120 m) are strongly influenced by soil thermal imbalance due to heat extraction, low thermal conductivity of the ground which leads to a soil temperature decrease in few years, and high drilling and installation costs [25,26]. Thereafter, horizontal GHEs that works in the shallow ground are favorable even if they need a greater soil surface for heat exchanger installation in order to overcome the lower thermal performance, due to soil temperature seasonal variations [27]. A possible further solution is to increase the

ground thermal conductivity to promote its heat storage and transfer capacity by adding backfilling materials around GHEs tube systems [28].

Most used backfilling materials are cement-based grouts, bentonite clay and sand, but between them, sand represents the cheapest material with higher thermal conductivity, which is usually around 1.3 W/m K, while bentonite thermal conductivity is around 0.7 W/m [29,30]. Although thermal conductivity has great relevance, to further enhance GHEs performance heat storage capacity of backfilling material must be considered too. Therefore, LHTES technology must be studied as a possible way to reach both these goals. Several studies investigated solution to overcome PCMs low thermal conductivity, through encapsulation or conductive solid filler addition (e.g. graphite, carbon fiber, nickel or copper) [31]. In this context organic PCMs, and among them paraffins, should be considered as additive to GHEs backfilling material, due to the fact that their melting and crystallization involves a large amount of latent heat [32–34]. In fact, paraffins are characterized by high reliability through phase change cycles, chemical stability, limited supercooling, absence of incongruent melting and relative low cost, when compared with other materials for similar application, while theirs major drawback is the extremely low thermal conductivity, which is usually between 0.1 and 0.3 W/m K [35,36].

Thereafter, as first innovative aspect of the present study, direct mixing of backfilling sand and paraffin was tested as a promising option to enhance the heat storage capacity of the former and thermal conductivity of the latter. In addition, to overcome the great soil surface needed and relative digging cost for horizontal GHEs, a novel Flat-Panel GHE architecture was considered [37], since its flat shape easily allows the backfilling into the installation trench. In fact, previous studies demonstrated that the addition of PCMs in the backfill sand would raise also the amount of heat stored in the area around the GHE, avoiding loss of thermal conductivity due to dispersion in soil [38]. In this context, the present study focuses on the interactions of two different organic PCMs, *n*-Octadecane paraffin and a paraffin-based commercial PCM, mixed with silica sand, combined to a flat shape representing the Flat-Panel GHE architecture. The comparison, through two sequentially groups of tests, was done in order to estimate the differences in terms of thermal performances and materials morphology between the two PCMs but also to evaluate their interactions with backfilling material undergoing to several heating/cooling cycles.

2. Materials and Methods

Two experiments, so called *Vials* and *Sand-box*, with different procedures, were carried out with the aim of investigating the thermal behavior of PCMs - sand mixtures and their possible integration of PCMs with sand,

respectively. Two organic PCMs were used for the experiments (Table 1). *n*-Octadecane paraffin ($C_{18}H_{38}$, 99%, CAS: 593-45-3) was purchased from *Alpha Aesar*, commercial grade paraffin wax PCM A28 was provided by *PCM Products Ltd (UK)*. Both PCMs have phase change temperatures at 28 °C [39–41]. Dry sand (S) was used in the composition of the mixture-samples for the experiments.

Table 1. PCMs properties

PCM	Melting Point (°C)	Density (kg/m^3)	Latent Heat (kJ/kg)	Specific Heat Capacity (kJ/kg K)	Thermal Conductivity (W/m K)
$C_{18}H_{38}$	28	776	241	2.0	0.33
A28	28	789	265	2.2	0.21

2.1 Vials Test

The thermal behaviors in time-temperature graphs of *n*-Octadecane (O), A28 and of their mixtures with dry sand, OS and AS respectively, were observed. Melting and freezing tests, supercooling and performance stability through thermal cycles were evaluated in a temperature range between 23 and 33 °C (ΔT=10 °C). Analysis tests were performed using "*Falcon*" vials (V= 55 ml) dipped into a *Thermo Scientific Haake A25/AC200* water bath circulator. In order to prepare OS and AS samples, sand and PCMs were mixed separately by manual mixing. Proportion among PCMs and sand was 30:100 in volume considering the average porosity of the sand. The PCMs mass ration between pure and mixture samples was about 1:4. The monitoring was carried out by using K-type thermocouples (ZA9020-FS, *Almemo*) connected to a data logger *Almemo 710,* (*AHLBORN*) with a resolution of 0.1 K and a linearization accuracy of ±0.05 K ±0.05% of the measured value. One thermocouple was centered inside each vial and a third thermocouple was dipped directly into water as reference (Figure 1).

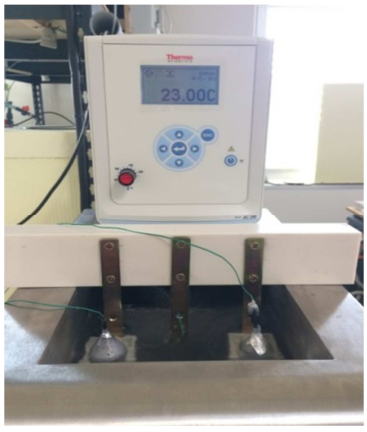

Figure 1. Falcon vials and reference in the cryostat bath

Initially, two consecutive melting-solidification cycles were obtained considering a condition of high thermal stress applied to the O and OS samples since they were brought instantly from T_{min} = 23 °C to T_{max} = 33 °C and vice versa, i.e. without gradual heating and cooling processes. For OS and AS, 16 solid-liquid-solid phase transition cycles were performed, following a programmed temperature ramp of 5 steps (Figure 2) in order to observe their thermal behavior over a relatively long period. Even for O and A28 samples one melting/solidification cycle was observed with a programmed temperature ramp as shown in Figure 2, in which the duration in minute is indicated for each step of the two different ramps.

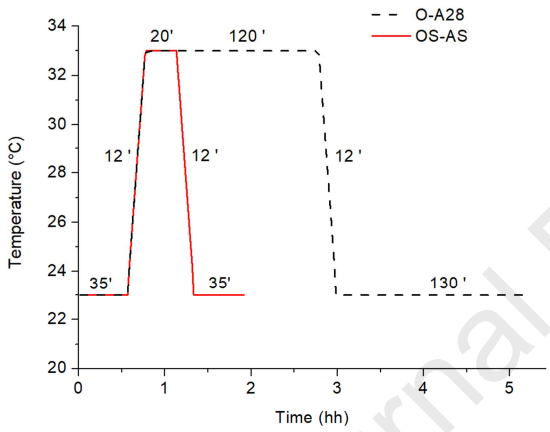

Step	O-A28		OS-AS	
	T(°C)	Time (min)	T(°C)	Time (min)
1	23	35	23	35
2	23-33	12	23-33	12
3	33	120	33	20
4	33-23	12	33-23	12
5	23	130	35	35

Figure 2. Programmed temperature ramps for O-A28 and OS-AS tests.

2.2 Sand-box test

Consequently, to *Vials test* results, A28 and AS were tested into a sand-box to better simulate realistic conditions of the mixture near the Flat-Panel GHE, with the purpose of consider direct mixing as a possible concrete solution for underground thermal energy storage (UTES). The experiment consists in comparing the thermal behavior of the same mass of pure PCM inside a container and its direct mixing with sand, under the same boundary conditions (Figure 3). The tests were carried out by heating and cooling samples in the same temperature range 23-33 °C. The tests were executed in a room at constant temperature around to 23 °C. The PCM was laid horizontally inside a sand-box in contact with a square thermal plate, an electrical resistance operating as a thermal source, placed at a fixed depth of 4 cm from the surface of the sand. A multi-range DC power supply *PSW 80-27, GWInstek* was connected to the electrical resistance inside the square plate in order to manage voltage and current and therefore the thermal power. Regarding

A28 sample, 14.8 g of PCM was set inside a rectangular polycarbonate container with the same thermal conductivity value of the PCM [42].

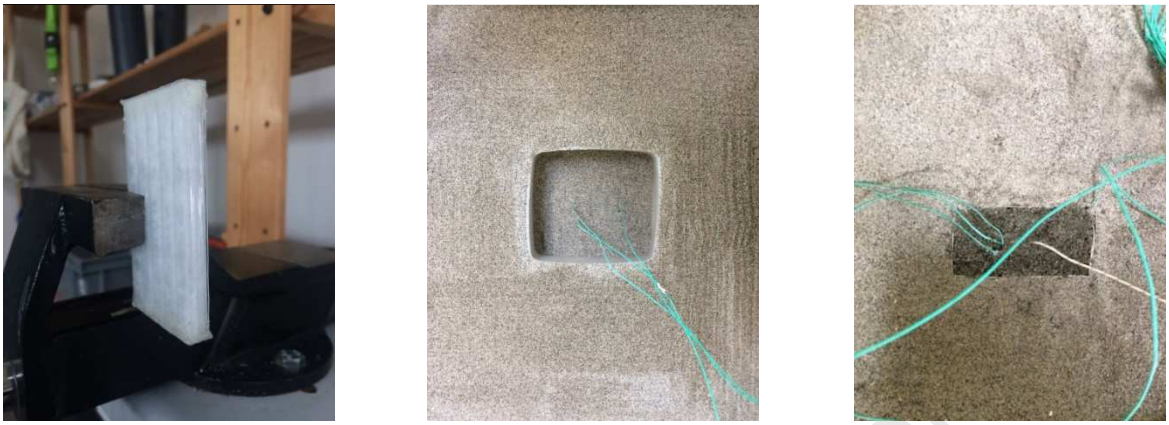

Figure 3. A28 inside the polycarbonate container (left), thermal plate placed inside sand (middle), and AS placed inside sand (right)

AS sample was prepared considering the average porosity of the sand and a mass equivalence of the PCM in reference to the mass of A28 inside the polycarbonate container. The mixture was in direct contact with the underside of the square thermal plate and with the sand on the other sides. Moreover, for both tests the condition of equivalent heat exchange surface was respected, hence the mixture was molded in order to have a shape and a contact surface (31.2 cm^2) with the thermal source similar to the one of the containers (Figure 3). Furthermore, a reference test was performed considering the sand-box without PCM. For the purposes of the tests, significant values of the masses, volumes, dimensions of the materials and instruments are listed in Table 2.

Table 2. Masses, volumes and dimensions of the materials and instruments used in the experiment.

	Dimension (cm)	**Heat transfer surface (cm^2)**	**Volume (cm^3)**	**Density (g/cm^3)**	**Mass (g)**
Thermal plate	12x12x0.2	144			
Sand-Box	38x38x32	1444	$46.2 \cdot 10^3$	1.625	$75 \cdot 10^3$
Polycarbonate container	7.8x4x0.8	31.2	18.7		5.10
A28 in container				0.789	14.8
AS	7.8x4x1.7	31.2	53.0		101
A28 in AS				0.789	14.8
S in AS			53.0	1.625	86.2

For installation needs, two different types of thermocouples connected to a data logger Almemo 710 (AHLBORN) and installed at a certain depth inside the sand-box were used. According to a better wiring flexibility and strength, K-type thermocouples (ZA9020-FS, Almemo) were installed at the lower side of the setup and never removed, whilst T-type

(ZA9021-FST, Almemo) were laid at upper side and removed every test. As reported in their data sheet (Almemo measuring instruments), both probes have a resolution of 0.1 K and a linearization accuracy of ±0.05 K ±0.05% of the measured value; however, T-type operates in a measuring range -200/+400 °C, while K-type -200/+1370 °C.

To check that the different type of thermocouples would not have affected the measured data, an experimental comparison was carried out by putting them into the thermal bath and monitoring for four cycles programmed in the temperature range of the PCM melting point (23-33°C). The maximum temperature difference was verified to be equal to 0.3K, therefore within the accuracy of both types, and always the T-type 0.2-0.3K warmer than the K-type. As a consequence, the accuracy has to be considered of the same range.

In Figure 4 are schematically represented the cross-section for A28 and AS tests. All thermocouples (K-type: green dots, T-type: red dots) were positioned at the same depths for all tests and defined by a letter in alphabet order starting from the deepest one. Taking into account the distance from sand-PCM interface, A, B, C and D is laid far 5, 3, 2 and 1 cm respectively. For A28 inside container the thermocouple E is located at the sand-PCM interface, while for AS test is 1 cm inside the mixture. Finally, F is between the square thermal plate and PCM, H 2 cm above the square thermal plate, and I at the sand surface.

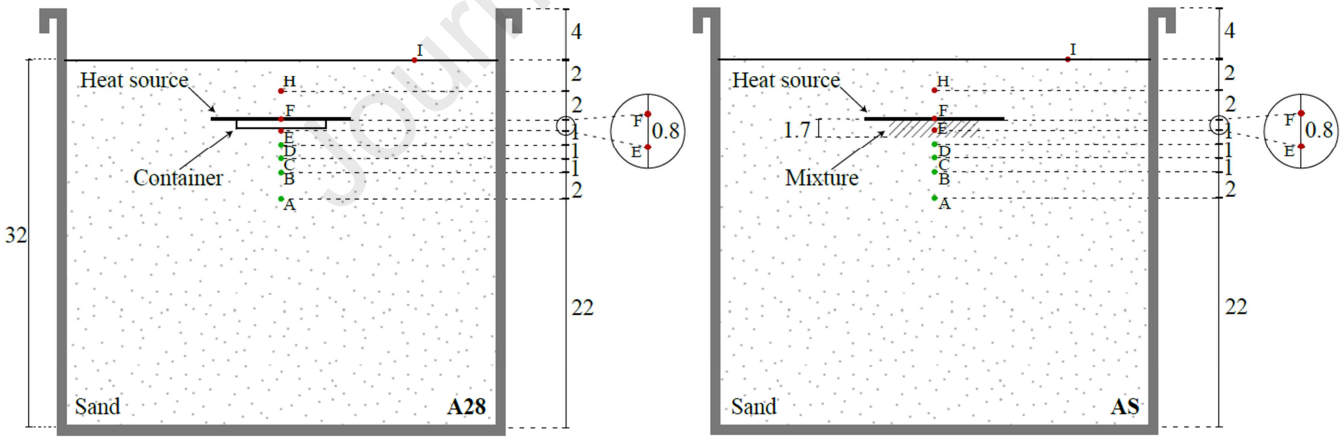

Figure 4. Cross-section of the sand-box containing A28 inside polycarbonate container (left) and AS (right)

The thermal plate provided a thermal power of ~ 2.9 W (I= 1.46 A, V=1.95 V). This power combined with the large mass of sand-box was able to maintain the heating plate at temperature of ~ 34 °C for the entire duration of the heating process (about 21 hours), thus allowing the solid-liquid phase change of the PCM. At the end of the heating process the DC power supply was turned off, triggering the relaxation of the system to the room temperature (23°C), and starting

the cooling process and consequently the solidification of the PCM (about 8 hours). The entire duration of the measurement cycle was of 29 hours, approximately.

2.3 Materials Characterizations

Structure of sand and mixtures was evaluated by semi-quantitative energy dispersive X-ray spectrometry (X-EDS, Oxford INCA-350) at room temperature. In addition, Fourier Transform Infrared Spectroscopy in ATR mode (FTIR Vertex 70, Bruker) was employed to collect information about chemical compositions and bonds reactivity. The FTIR-ATR spectra were obtained in the range of 600–4000 cm^{-1}, with 4 cm^{-1} resolution and 30 scans at room temperature (25 °C). The thermal behavior of each sample was measured using DSC analysis (TA instruments, 2010 DSC) performed in air at the heating rate of 1°C/min. The DSC measurements were carried out on *ca.* 40 mg of sample in an aluminum crucible. The error on such a measurement is equal to the sensitivity of the instrument (1°C). Morphology was investigated through environmental scanning electron microscopy (ESEM, Quanta 200) and grain size laser diffraction (Mastersizer 2000 Hydro, Malvern Instruments) in distilled water to investigate grains dimension and their distribution in pure sand and sand-PCMs mixtures. All the grain size measurements were performed after sonication to avoid aggregates formation and the curves reported are the average of a total of 10 measurement for each sample, instrument sensibility is equal to 1 µm. Pore distribution and its variations between samples were evaluated through mercury intrusion pore measurement (Autopore IV 9500, Micromeritics) at room temperature employing a mercury filling pression equal to 1.51 psia, and an equilibration time of 10 s. The values obtained are representative of the average of 5 measurement on the same sample, instrument sensibility is equal to 3.6 µm. Physical properties investigation was carried out at room temperature through optical microscopy (M125C, Leica) and absolute density measurement through helium pycnometer (Accupyc II 1330, Micromeritics) having instrument sensibility of 0.0001 g/cm^3. Each reported value is the average of a set of 10 measurements on the same sample.

3. Results and Discussion

3.1 Dry sand (S) characterization

As shown in Figure 5 sand (S) presents great variability in grain size moving from 250 to 700 µm. Despite this, d0.5 of the gaussian distribution is near to 358.9 µm, that can be considered as representative of a large amount of grains, considering the strong symmetry of the grain size distribution. The grain size analysis is confirmed through optical (Figure 6a) and ESEM observation (Figure 6b). Pore size measurement, through mercury intrusion, highlights that the

majority of pores has a size between 26 and 30 µm (Figure 7), and the absolute density measured through Helium pycnometer detected a density equal to 2.7251 ± 0.0008 g/cm^3 (Figure 8).

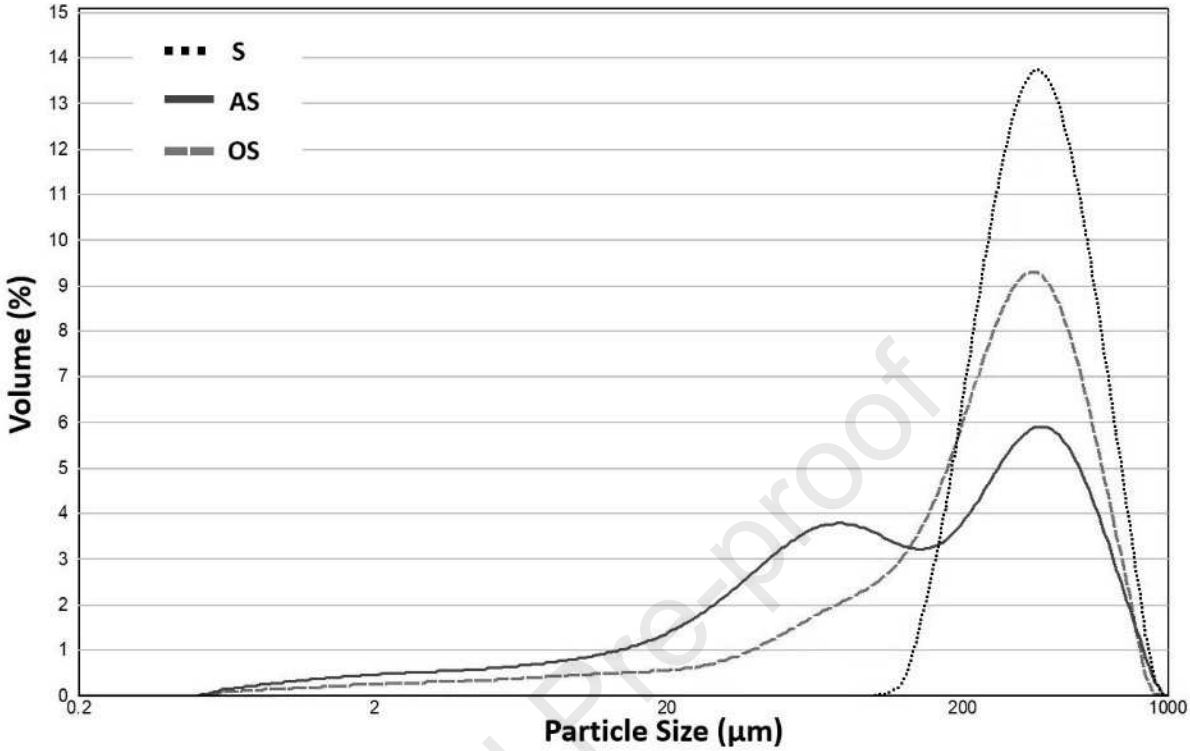

Figure 5. Particle size distribution of sand (S) and mixtures after *Vials* test

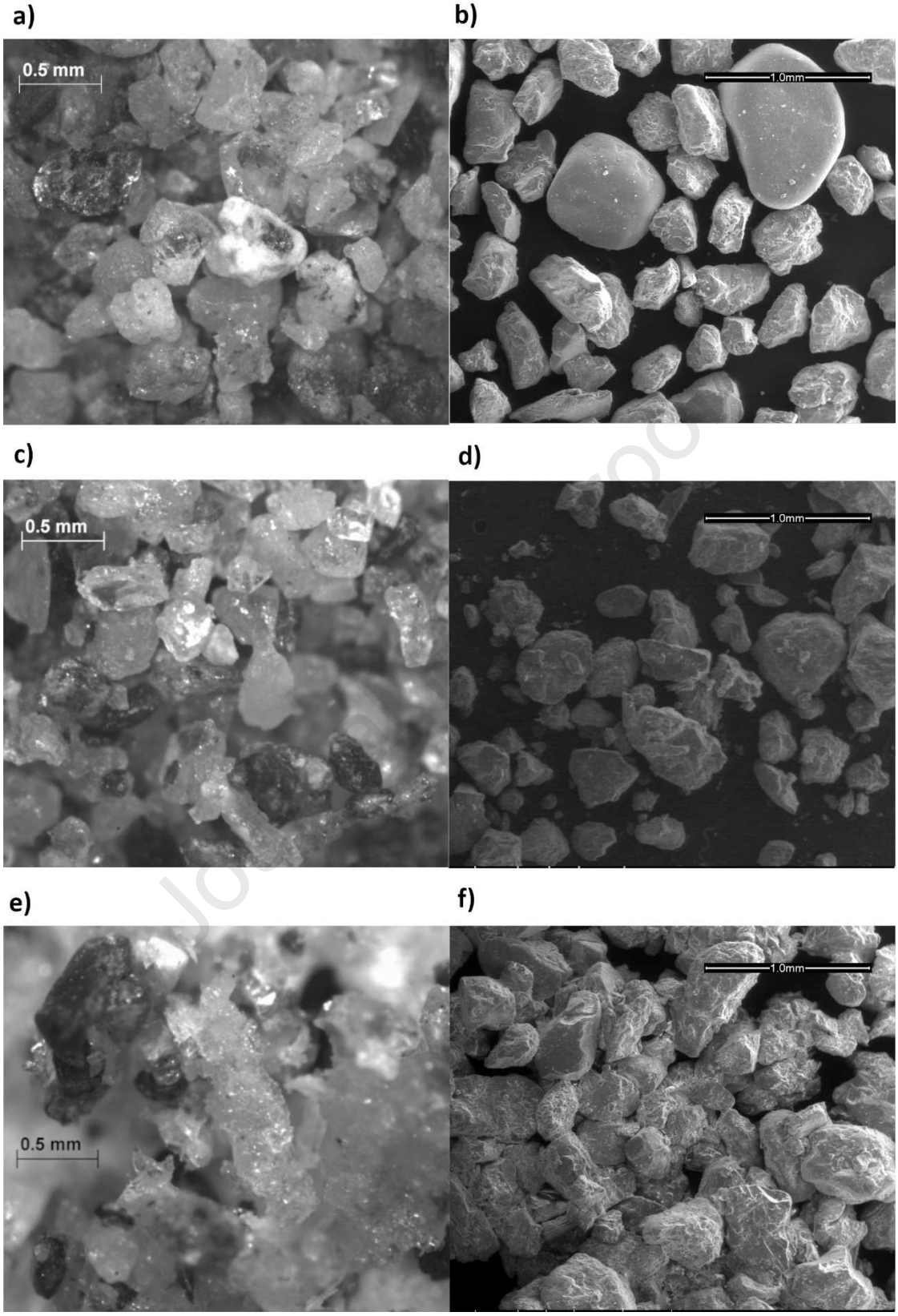

208

209 Figure 6. Microscopies before and after *Vials* test: a) S under optical observation at 35X, b) S under ESEM observation
210 at 100X, c) AS under optical observation at 35X, d) AS under ESEM observation at 100X, e) OS under optical
211 observation at 35X f) OS under ESEM observation at 100X.

212

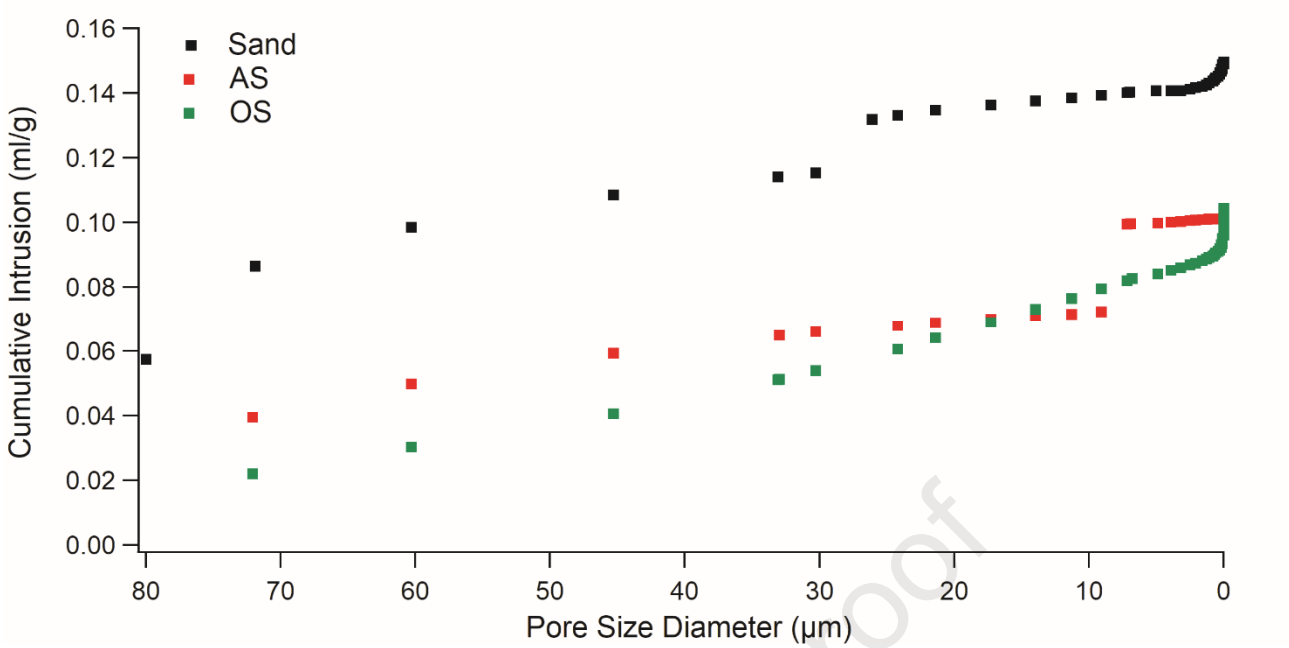

Figure 7. Pore size measurement performed on S, AS and OS after *Vials* Test

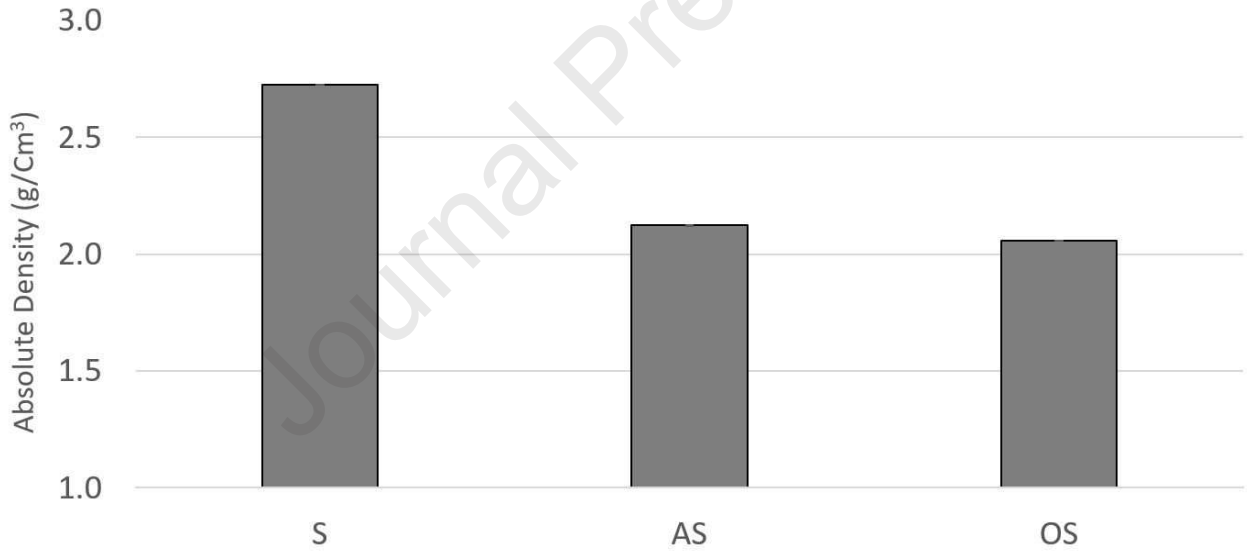

Figure 8. Absolute densities after *Vials* Test (Error bars are reported but too small to be visible)

As expected, EDS (Figure 9) and FTIR (Figure 10) techniques detected a great variability of the semi-quantitative chemical composition with the presence of local areas enriched in metal. This is consistent with the technical grade of S and confirmed through optical microscopy observation. X-EDS analysis (Figure 9) performed in three different regions of the grains has highlighted the presence of silicon (around 80 wt %) and aluminum (around 19.4 wt %), two elements typically in great quantity into silica sands, with local spots enriched in calcium (around 80 wt %) and iron (around 20%). These results are consistent with FTIR analysis (Figure 10): silicon presence is confirmed by the broad peak with a maximum around 1000-990 cm^{-1} that corresponds to Si-O-Si and Si-O stretching bonds, but also by the peak at 776

226 cm^{-1} [43]. Finally, the sharp peaks at 716 cm^{-1} correspond to C-O bonds indicating a possible inclusion of organic
227 content [44].

228

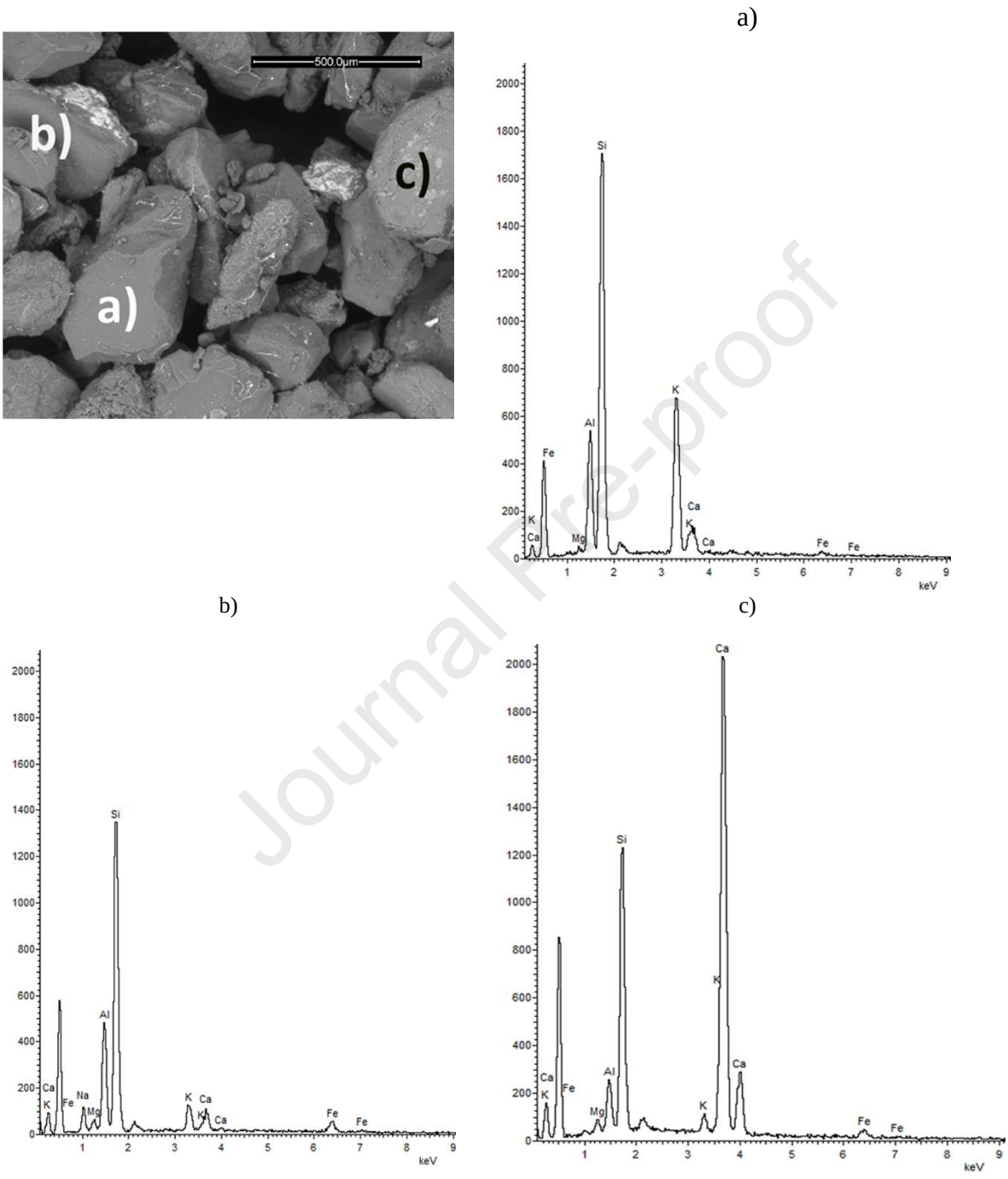

229

230 Figure 9. EDS spectra of S that highlight the presence of different elements in different regions of interest of the sample
231

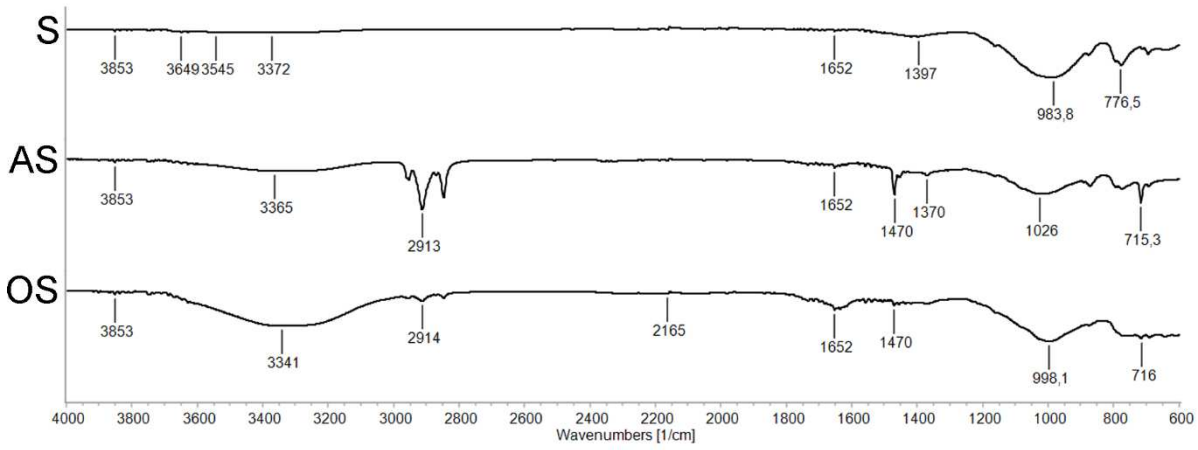

Figure 10. FTIR spectra after *Vials* Test analysis

3.2 Vials test analysis

Considering the two consecutive heating/cooling cycles test for O and OS samples (Figure 11a) the phase change time ratio between the two samples is estimated from the ratio $\Delta t_2/\Delta t_1$ measured taking as reference the trace of the bath and the time values. References of O and OS have been taken traces at a temperature of 30.5 °C (Figure 11b), chosen as intermediate value between the melting point of the PCM and the maximum working temperature (T = 33°C). This time ratio is about 1:8 while the PCM mass ratio is 1:4. Therefore, the phase change is not only related to the mass of the PCM but is also influenced by the mass of the sand which provides a significant contribution to the celerity of heat transfer thanks to its high thermal conductivity and heat capacity compared to the PCM ones.

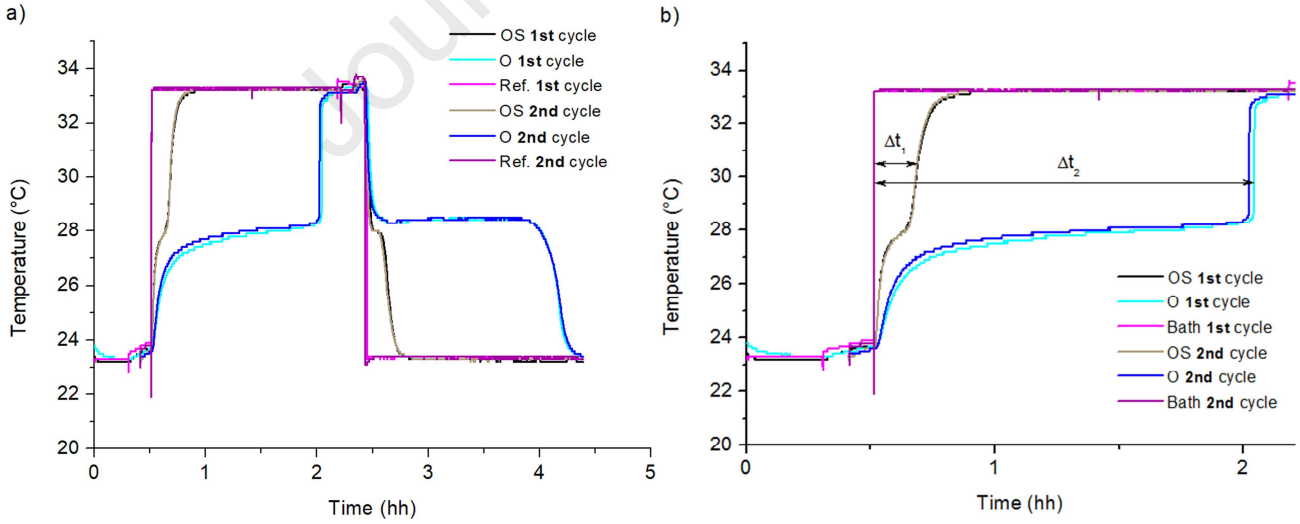

Figure 11. a) Overlap between two phase transition cycles. b) Δt phase transitions comparison during the heating process.

In Figure 12a, it can be observed that the overall temperature trends of A28 and O is quite similar, and supercooling is never evident, according to their chemical nature. Moreover, the phase change is well highlighted by a horizontal trend around 28°C. In Figure 12b and 12c the comparison between the first and the sixteenth thermal cycles for OS and AS

show how sand affects functionally the PCMs. The difference in masses between O, A28 and OS, AS samples is substantial, nevertheless the sand greatly enhances the thermal conductivity of the mixture. OS showed a slight supercooling (~1°C) during the solidification process, which is not shown by O (Figure12a); therefore, it has to be correlated to the PCM-sand interaction. The same is observed in AS test, albeit in a not evident way as the supercooling is barely noticeable probably due to the different chemical composition. Despite having both a paraffin nature, O has a defined composition (*n*-Octadecane, 99%) while A28 is a commercial grade paraffin wax and its composition is not specified in the datasheet, although it may be assumed to be an organic eutectic. The reason why the supercooling phenomenon was observed only in the mixture samples is not yet well cleared, and consequently it will be the subject of further studies.

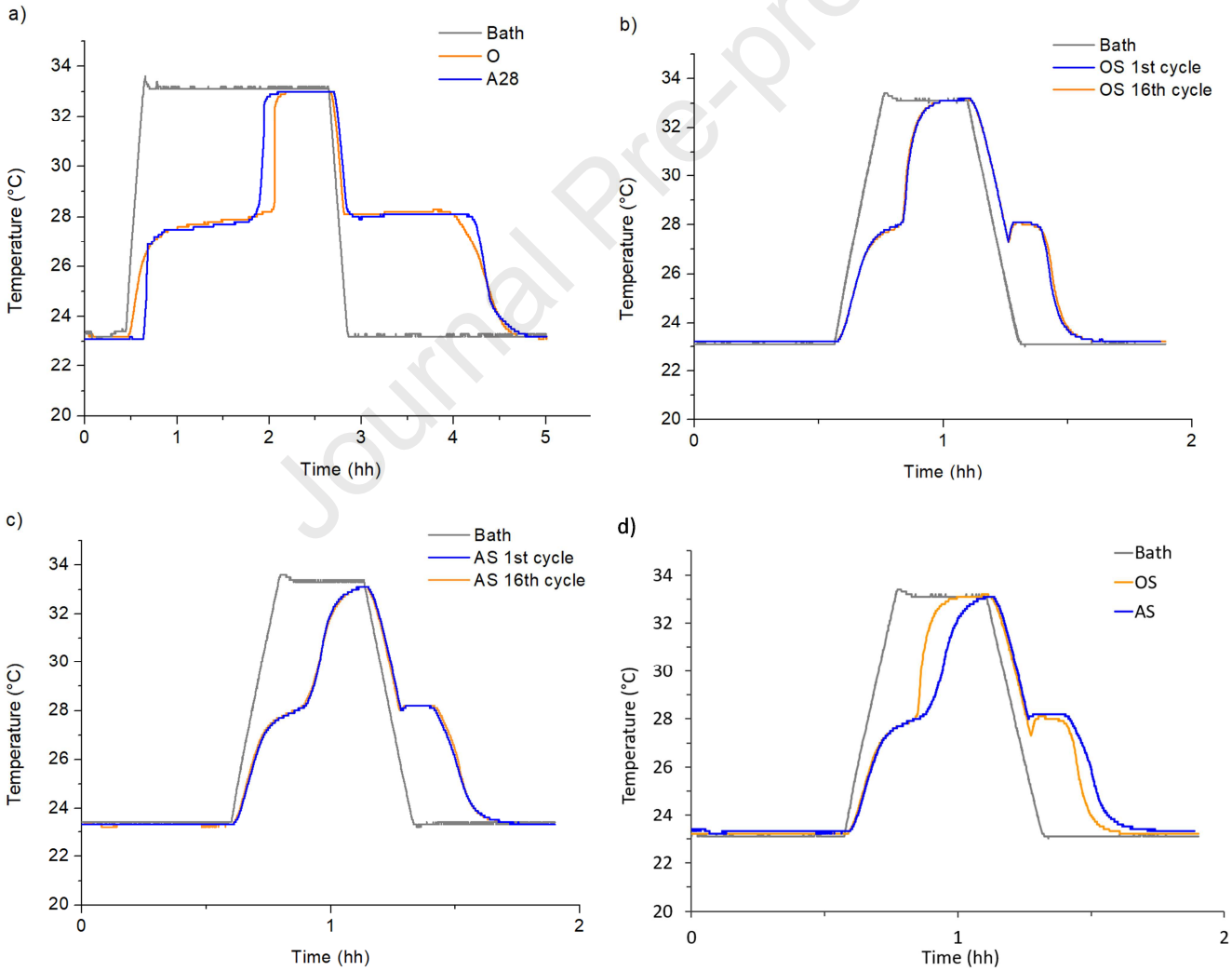

Figure 12. Temperature cycle overlaps: O-A28 (a), 1st and 16th OS (b), 1st and 16th AS (c), and OS-AS (d).

3.3 Comparison among S, and S- PCM mixtures after Vials Test

The increasing thermal cycles number affected PCM-sand mixtures structural properties in different ways. For first, grain size measurement (Figure 5) detected a reduction with respect to S. Bimodal gaussian curves represent AS and OS samples strongly moving the average grain size to lower dimension with respect to S. Almost 25 % of particles of OS mixture has diameters lower than 120 µm, while for AS sample the percentage under 120 µm is near to 47 %. Again, this data is confirmed by the optical microscopy and ESEM analysis (Figure 6) that shows particles with dimensions from 50 to 700 µm for AS (Figure 6c and 6d), quite similar to OS (Figure 6e and 6f) showing particles from 30 to 600 µm. This result is due to the friction of the particles during the thermal cycles, considering that PCM melting and freezing affect the volume among sand particles, and thereafter the total volume of the mixtures. OS and AS, show also a pore size decrease respect to S, but while OS sample shows a general drop in the range from 30 µm to less than 1 µm, AS is characterized by generation of smaller pores in a narrow range between 7 and 9 µm (Figure 7). Again, pores reduction indicates that a mechanical action among particle occurs, breaking the greater pores, leading to a reduction of the grain size, and leaving only lower pores that are probably less easy to break, because better surrounded by the grain structure. This action also effects the volume among particle that can be seen in relevant decreasing moving from S to OS or AS (Figure 7). In fact, in this figure each curve is divided in two parts, the first from the origin to the flat section, regarding the interparticle volume, whereas the second attributed to the open porosity. The reduction of interparticle volume is certainly due to PCM addition to sand that during melting-freezing cycles (or solid-liquid transitions) is able to occupy this volume, adapting to different space geometry. Physical properties of samples were influenced by cycle number as well, in particular an absolute density decreasing can be observed for AS and OS, with respect to S, leading to an absolute density which is almost the same for OS and AS (respectively 2.0571 ± 0.0004 and 2.1220 ± 0.0002 g/cm^3). Absolute density decreasing is certainly due to PCM addition that has in general lower density with respect to sand. In addition, PCMs' action leads to a fragmentation of sand grains and consequently to an increase of sample total volume. As shown from optical microscopy and ESEM (Figure 6), *n*-Octadecane and A28 cover sand's grain with a thin film. It is interesting to observe with the optical microscope that this layer seems to reflect light, and difference among A28 and *n*-Octadecane can be detected. In particular, OS samples shows phase separation between sand and *n*-Octadecane, whose clusters are visible in Figure 6e. AS instead shows no phase separation and A28 is located mainly in the contact points between grains (Figure 6c). These differences can be connected with the different response in terms of thermal cycling measurement leading to AS samples the more promising results in terms of thermal conductivity by enhancing a stronger physical connection with sand. Thereafter, also some consideration about the structure of the mixtures have been made through FTIR technique to investigate difference among OS and AS samples and related to

PCMs addition as shown in Figure 10. For samples AS, and OS, the band in the range 3500-3000 cm^{-1} is due to –OH bond stretching vibration [45,46], the broad band indicates that there are different bonding states of OH groups, meaning that there is as strong and broad bonding due to hydroxyl group among paraffins and sand after thermal cycling [43]. This band is one of the principals for OS sample. In strong similarity the sharp peak at 1470 is due to C-H bond detriment. Thereafter connection between PCMs and sand are mainly driven by C-H bonds reduction and -OH bond increasing. For sample AS three sharp peaks at 2953, 2913 and 2848 cm^{1}, can be detected, which correspond respectively to asymmetric $–CH_3$, asymmetric $–CH_2–$ and symmetric $–CH_2–$ bonds stretching vibration [46]. These peaks are mainly not present for OS indicating that $–(CH)_n-$ groups are not relevant for *n*-Octadecane-sand mixture. Whereas for OS, the broad peak at 1652 cm^{-1} is due to the stretching of aliphatic (alkene) C=C bond [43]. Difference among OS and AS samples have been detected and thereafter different type of bonding can be attributed to the different behavior of OS and AS mixtures.

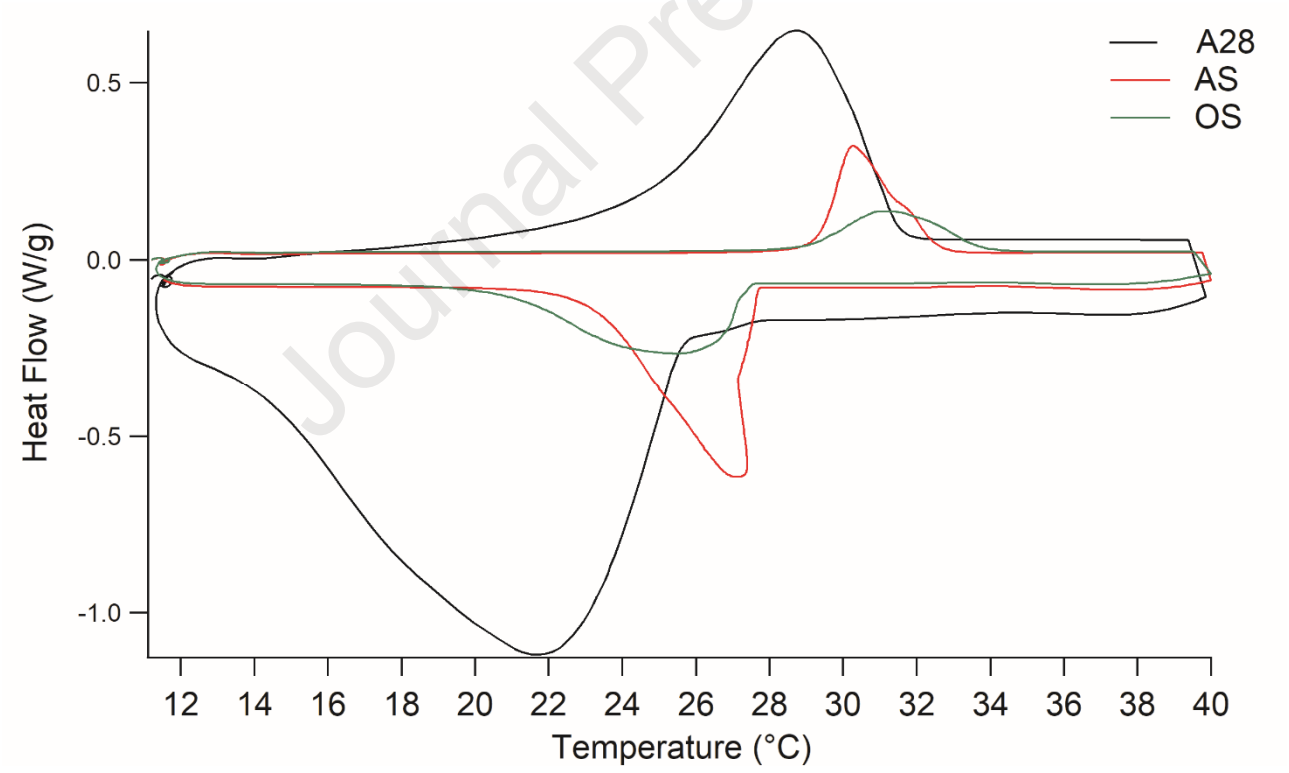

Figure 13. DSC analysis of A28, AS and OS samples

Finally, a thermal analysis (DSC) has been conducted on pure A28, AS and OS samples as reported in Figure 13. This analysis shows that melting temperature for pure A28 (exothermic peak) is completely consistent with the data obtained from the supplier (Table 1) and is equal to 28 °C. Mixture of A28 with sand (AS) lead to a slight increase of the melting

temperature, near to 30°C and to a decreasing of the latent heat (area below the exothermic peak) as expected, due to the fact that sand is added to a PCM. A very different behavior con be observed for OS samples when compared to AS, with a further increasing of the melting temperature, near to 31 °C and a reduction of the latent heat, as results of a lower and broader exothermic peak. This result is consistent with the fact that $C_{18}H_{38}$ latent heat is lower than A28 one (Table 1).

3.4 Sand-box test analysis

Consequently, to *Vials test* results, demonstrating good thermal performance avoiding supercooling effect, A28 and its mixture with sand were chosen for further analysis through *sand-box*. From A28 and AS tests in *sand-box*, it was possible to analyses how the heat transfer occurs in sand under the same boundary conditions (heating power, environmental temperature, …), but with different ways of PCM coupling. Figure 13 shows three normalized temperature graphs respectively of the polycarbonate container filled with A28, AS and pure sand (reference case), by using equivalent thermocouples for a more direct and prompter comparison (A, B, C, D, F, H). The Y axis reports normalized temperature values obtained by considering the respective ΔT between the temperature values actually measured by the thermocouples shown in the graphs and their initial value of the test. Normalization is proposed in order to fix some temperature discrepancies of about 0.8-1.2°C of the initial temperatures measured by the thermocouples at the starting of the heating/cooling cycle, which occurred between the three tests and referable to environmental room temperature. Indeed, the starting temperature of the tests coincides with the room temperature, which during the various days reserved for the completion of the 3 cycles underwent slight variations that influenced the initial temperatures detected by the thermocouples between one test and the others. Regarding the thermocouples F (PCM-Source interface) it should be noted that for both tests concerning the PCM their behavior is temporally comparable and related to the PCM effect. The temperature measured by the thermocouple H show a higher value for A28 in polycarbonate, therefore the latter creates a higher thermal resistance due to the lower thermal conductivity of pure PCM A28 with respect to the AS blend. Furthermore, this is also depicted by the thermocouples positioned deeper in the sand (A, B, C, D). When testing A28 inside container the temperatures detected by these sensors are lower than the analogue ones for the AS test. Indeed, the thermal source exchanges more heat upward than downward, and this explains why the thermocouples H reaches higher temperature values as well. On the other hand, AS case allows to improve the heat transfer, drastically decreasing the thermal resistance of pure PCM with the higher thermal conductivity of the sand. This behavior could be further justified by the shorter duration of the phase transitions during heating/cooling processes, because of the same PCM mass, the different time in melting should be related to a different heat flux occurring in the domain, higher downward than upward for AS with respect to A28 inside container. In AS

graph it can be noticed the same slight supercooling phenomenon already monitored during the *Vial-test* (Figure 12c), probably due to an interaction between sand and A28 to be furtherly deepen.

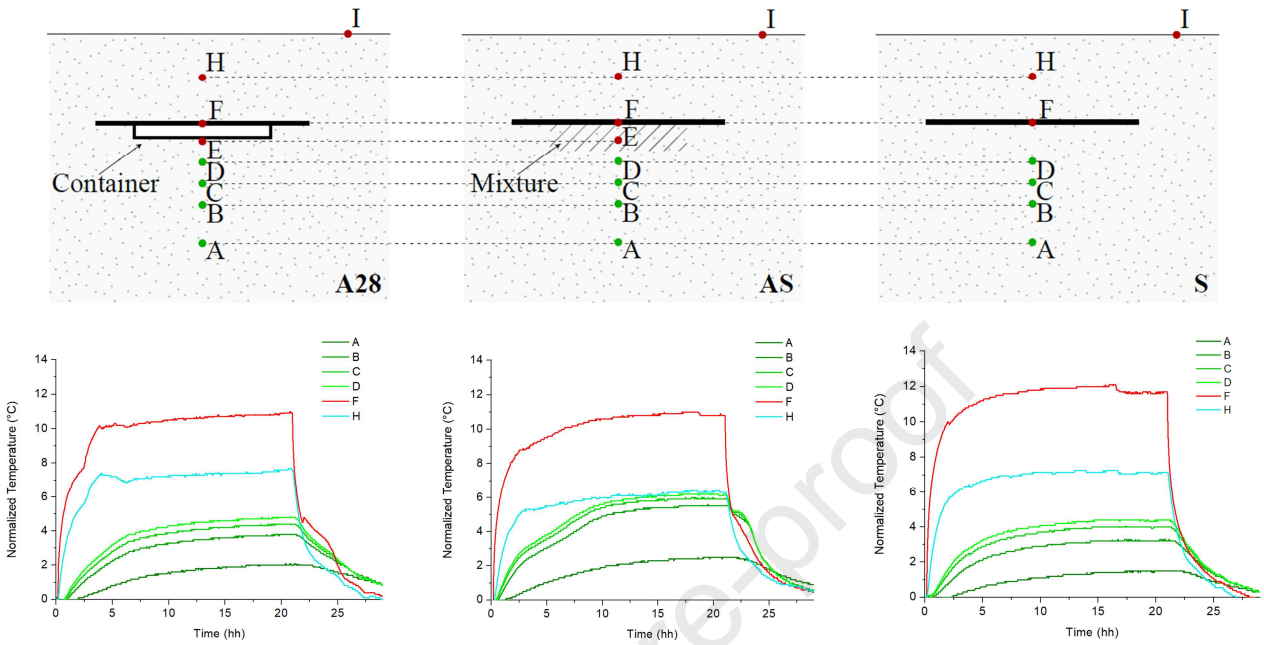

Figure 14. Comparison of the temperature time trends detected by the A, B, C, D, F, H thermocouples for the three tests: A28 (left), AS (middle), and S (right)

4. Conclusions

In this work, the employment of two organic PCMs, *n*-Octadecane and commercial paraffin A28, mixed with common silica sand was evaluated to perform distributed LHTES coupled with a novel shape of shallow ground GHE (so called Flat-Panel). Melting and freezing rates of pure PCMs and PCM-sand mixtures were compared, while their variation with phase change cycles number was evaluated too. By testing in thermal bath (*Vial test*), it was noted that the presence of the sand promotes the celerity of the heat transfer phenomenon, since a sample with a mass ratio of 3/4 of sand and 1/4 of PCM needed around 11' for melting unlike almost 90' for the sample with 4/4 of PCM. These enhancements remain constant with increasing thermal cycles number, while physical properties change, in particular a reduction in grain (from 358 µm to below 120 µm) and pore size (from 30 µm to below 1 µm) was detected and attributed to mechanical friction among particles. For the same reason, a decrease in absolute density was highlighted (-3 %), while sand and PCMs composition remained constant through cycles. Commercial PCM A28, resulting the more interesting after *Vials test*, was further tested in more realistic conditions (*Sand-box test*), with the same PCM mass and conditions. In this set-up, the direct mixing case (PCM & sand) increased the filed temperature below the heating plate of more than 1 K, when compared to the case in which the same mass of PCM was constrained inside a container.

Despite changes in structural and physical properties of the mixtures, thermal performances remained constant through cycles, demonstrating the feasibility of direct mixing of silica sand and organic PCMs for distributed LHTES coupled with shallow ground GHE.

Funding

This study was funded by the Emilia Romagna region in the framework of the project "CLIWAX" co-financed by 2014-2020 POR FESR Emilia-Romagna Region Italy DGR 774/2015 – CUP F71F18000160009 and the project "IDEAS" financed by the European Union's Horizon 2020 research and innovation program, G.A. No. 815271. The authors declare that there is no conflict of interests.

References

[1] P. Dean, B., Dulac, J., Petrichenko, K., and Graham, Towards a zero-emission, efficient, and resilient buildings and construction sector, United Nations, 2016.

[2] European Parliament, DIRECTIVE (EU) 2018/844 OF THE EUROPEAN PARLIAMENT AND OF THE COUNCIL of 30 May 2018 amending, Off. J. Eur. Union. (2018).

[3] European Parliament, DIRECTIVE 2010/31/EU OF THE EUROPEAN PARLIAMENT AND OF THE COUNCIL of 19 May 2010 on the energy performance of buildings, Off. J. Eur. Union EN L. (2010) 23.

[4] IEA, Tracking Buildings, Paris. (2019).

[5] U. Stritih, V. V. Tyagi, R. Stropnik, H. Paksoy, F. Haghighat, M.M. Joybari, Integration of passive PCM technologies for net-zero energy buildings, Sustain. Cities Soc. 41 (2018) 286–295. doi:10.1016/j.scs.2018.04.036.

[6] A. Sharma, V. V. Tyagi, C.R. Chen, D. Buddhi, Review on thermal energy storage with phase change materials and applications, Renew. Sustain. Energy Rev. 13 (2009) 318–345. doi:10.1016/j.rser.2007.10.005.

[7] Y. Jemmal, N. Zari, M. Maaroufi, Thermophysical and chemical analysis of gneiss rock as low cost candidate material for thermal energy storage in concentrated solar power plants, Sol. Energy Mater. Sol. Cells. 157 (2016) 377–382. doi:10.1016/j.solmat.2016.06.002.

[8] R. Stropnik, R. Koželj, E. Zavrl, U. Stritih, Improved thermal energy storage for nearly zero energy buildings with PCM integration, Sol. Energy. 190 (2019) 420–426. doi:10.1016/j.solener.2019.08.041.

[9] P.K.S. Rathore, S.K. Shukla, Potential of macroencapsulated pcm for thermal energy storage in buildings: A comprehensive review, Constr. Build. Mater. 225 (2019). doi:10.1016/j.conbuildmat.2019.07.221.

[10] M. Iten, S. Liu, A. Shukla, A review on the air-PCM-TES application for free cooling and heating in the buildings, Renew. Sustain. Energy Rev. 61 (2016) 175–186. doi:10.1016/j.rser.2016.03.007.

[11] L.F. Cabeza, L. Navarro, A.L. Pisello, L. Olivieri, C. Bartolomé, J. Sánchez, S. Álvarez, J.A. Tenorio, Behaviour of a concrete wall containing micro-encapsulated PCM after a decade of its construction, Sol. Energy. (2019) 0–1. doi:10.1016/j.solener.2019.12.003.

[12] K.O. Lee, M.A. Medina, X. Sun, X. Jin, Thermal performance of phase change materials (PCM)-enhanced cellulose insulation in passive solar residential building walls, Sol. Energy. 163 (2018) 113–121. doi:10.1016/j.solener.2018.01.086.

[13] T. Silva, R. Vicente, F. Rodrigues, A. Samagaio, C. Cardoso, Performance of a window shutter with phase change material under summer Mediterranean climate conditions, Appl. Therm. Eng. 84 (2015) 246–256. doi:10.1016/j.applthermaleng.2015.03.059.

[14] S.S. Chandel, T. Agarwal, Review of current state of research on energy storage, toxicity, health hazards and commercialization of phase changing materials, Renew. Sustain. Energy Rev. 67 (2017) 581–596. doi:10.1016/j.rser.2016.09.070.

[15] A. Kylili, P.A. Fokaides, Life Cycle Assessment (LCA) of Phase Change Materials (PCMs) for building applications: A review, J. Build. Eng. 6 (2016) 133–143. doi:https://doi.org/10.1016/j.jobe.2016.02.008.

[16] Y. Li, N. Zhang, Z. Ding, Investigation on the energy performance of using air-source heat pump to charge PCM storage tank, J. Energy Storage. 28 (2020) 101270. doi:10.1016/j.est.2020.101270.

[17] E. Bonamente, A. Aquino, F. Cotana, A PCM Thermal Storage for Ground-source Heat Pumps: Simulating the System Performance via CFD Approach, Energy Procedia. 101 (2016) 1079–1086. doi:10.1016/j.egypro.2016.11.147.

[18] N. Zhu, P. Hu, Y. Lei, Z. Jiang, F. Lei, Numerical study on ground source heat pump integrated with phase change material cooling storage system in office building, Appl. Therm. Eng. 87 (2015) 615–623.

doi:https://doi.org/10.1016/j.applthermaleng.2015.05.056.

[19] E. Bonamente, Environmental Performance of Innovative Energy Storage, (2019).

[20] M. Dardir, K. Panchabikesan, F. Haghighat, M. El Mankibi, Y. Yuan, Opportunities and challenges of PCM-to-air heat exchangers (PAHXs) for building free cooling applications—A comprehensive review, J. Energy Storage. 22 (2019) 157–175. doi:10.1016/j.est.2019.02.011.

[21] E. Bigaila, A.K. Athienitis, Modeling and simulation of a photovoltaic/thermal air collector assisting a façade integrated small scale heat pump with radiant PCM panel, Energy Build. 149 (2017) 298–309. doi:10.1016/j.enbuild.2017.05.045.

[22] R. Lazzarin, M. Noro, Photovoltaic/Thermal (PV/T)/ground dual source heat pump: Optimum energy and economic sizing based on performance analysis, Energy Build. 211 (2020) 109800. doi:10.1016/j.enbuild.2020.109800.

[23] J. Yao, H. Xu, Y. Dai, M. Huang, Performance analysis of solar assisted heat pump coupled with build-in PCM heat storage based on PV/T panel, Sol. Energy. 197 (2020) 279–291. doi:10.1016/j.solener.2020.01.002.

[24] A. Mustafa Omer, Ground-source heat pumps systems and applications, Renew. Sustain. Energy Rev. 12 (2008) 344–371. doi:10.1016/j.rser.2006.10.003.

[25] T. You, W. Wu, W. Shi, B. Wang, X. Li, An overview of the problems and solutions of soil thermal imbalance of ground-coupled heat pumps in cold regions, Appl. Energy. 177 (2016) 515–536. doi:10.1016/j.apenergy.2016.05.115.

[26] Y. Wu, G. Gan, R.G. Gonzalez, A. Verhoef, P.L. Vidale, Prediction of the thermal performance of horizontal-coupled ground-source heat exchangers, Int. J. Low-Carbon Technol. 6 (2011) 261–269. doi:10.1093/ijlct/ctr013.

[27] M. Habibi, A. Hakkaki-Fard, Evaluation and improvement of the thermal performance of different types of horizontal ground heat exchangers based on techno-economic analysis, Energy Convers. Manag. 171 (2018) 1177–1192. doi:10.1016/j.enconman.2018.06.070.

[28] L. Liu, G. Cai, X. Liu, S. Liu, A.J. Puppala, Evaluation of thermal-mechanical properties of quartz sand–bentonite–carbon fiber mixtures as the borehole backfilling material in ground source heat pump, Energy Build. 202 (2019) 109407. doi:10.1016/j.enbuild.2019.109407.

[29] Y.A. Kara, Experimental performance evaluation of a closed-loop vertical ground source heat pump in the heating mode using energy analysis method, Int. J. Energy Res. 31 (2007) 1504–1516. doi:10.1002/er.1316er.

[30] D. Pahud, B. Matthey, Comparison of the thermal performance of double U-pipe borehole heat exchangers measured in situ, 33 (2001) 503–507.

[31] Y. Lin, Y. Jia, G. Alva, G. Fang, Review on thermal conductivity enhancement, thermal properties and applications of phase change materials in thermal energy storage, Renew. Sustain. Energy Rev. 82 (2018) 2730–2742. doi:10.1016/j.rser.2017.10.002.

[32] W. Yang, R. Xu, B. Yang, J. Yang, Experimental and numerical investigations on the thermal performance of a borehole ground heat exchanger with PCM backfill, Energy. 174 (2019) 216–235. doi:10.1016/j.energy.2019.02.172.

[33] D. Qi, L. Pu, F. Sun, Y. Li, Numerical investigation on thermal performance of ground heat exchangers using phase change materials as grout for ground source heat pump system, Appl. Therm. Eng. 106 (2016) 1023–1032. doi:10.1016/j.applthermaleng.2016.06.048.

[34] F. Chen, J. Mao, C. Li, P. Hou, Y. Li, Z. Xing, S. Chen, Restoration performance and operation characteristics of a vertical U-tube ground source heat pump system with phase change grouts under different running modes, Appl. Therm. Eng. 141 (2018) 467–482. doi:10.1016/j.applthermaleng.2018.06.009.

[35] H. Akeiber, P. Nejat, M.Z.A. Majid, M.A. Wahid, F. Jomehzadeh, I. Zeynali Famileh, J.K. Calautit, B.R. Hughes, S.A. Zaki, A review on phase change material (PCM) for sustainable passive cooling in building envelopes, Renew. Sustain. Energy Rev. 60 (2016) 1470–1497. doi:10.1016/j.rser.2016.03.036.

[36] R.K. Sharma, P. Ganesan, V. V. Tyagi, H.S.C. Metselaar, S.C. Sandaran, Developments in organic solid-liquid phase change materials and their applications in thermal energy storage, Energy Convers. Manag. 95 (2015) 193–228. doi:10.1016/j.enconman.2015.01.084.

[37] M. Bottarelli, M. Bortoloni, Y. Su, On the sizing of a novel Flat-Panel ground heat exchanger in coupling with a dual-source heat pump, Renew. Energy. 142 (2019) 552–560. doi:10.1016/j.renene.2019.04.088.

[38] J. Cao, M. Bottarelli, M. Bortoloni, G. Pei, Small-scale lab analysis of the ground freezing effect on the thermal performance of a Flat-Panel ground heat exchanger, Geothermics. 74 (2018). doi:10.1016/j.geothermics.2018.03.013.

461 [39] PCM Products Ltd, PlusICE Organic (A) Range, (2018).

462 [40] M. Azad, D. Dineshan, D. Groulx, A. Donaldson, N. Scotia, Melting of Phase Change Materials in a Cylindrical
463 Enclosure : Parameters Influencing, Proc. 4th Int. Forum Heat Transf. IFHT2016. (2016) 1–6.

464 [41] ThermoFisher scientific, Safety data sheet, (2018).

465 [42] Netzsch, Polycarbonate — Thermal Conductivity, (2020). https://www.netzsch-thermal-
466 analysis.com/en/materials-applications/polymers/polycarbonate-thermal-conductivity/.

467 [43] A.S. Khan, H. Khalid, Z. Sarfraz, M. Khan, J. Iqbal, N. Muhammad, M.A. Fareed, I.U. Rehman, Vibrational
468 spectroscopy of selective dental restorative materials, Appl. Spectrosc. Rev. 52 (2017) 507–540.
469 doi:10.1080/05704928.2016.1244069.

470 [44] M. Galván-Ruiz, J. Hernández, L. Baños, J. Noriega-Montes, M.E. Rodríguez-García, Characterization of
471 Calcium carbonate, calcium oxide, and calcium hydroxide as starting point to the improvement of lime for their
472 use in construction, J. Mater. Civ. Eng. 21 (2009) 694–698. doi:10.1061/(ASCE)0899-1561(2009)21:11(694).

473 [45] Y. Yang, W. Kong, X. Cai, Solvent-free preparation and performance of novel xylitol based solid-solid phase
474 change materials for thermal energy storage, Energy Build. 158 (2018) 37–42.
475 doi:10.1016/j.enbuild.2017.09.096.

476 [46] W. Wainipee, D.J. Weiss, M.A. Sephton, B.J. Coles, C. Unsworth, R. Court, The effect of crude oil on arsenate
477 adsorption on goethite, Water Res. 44 (2010) 5673–5683. doi:10.1016/j.watres.2010.05.056.

478

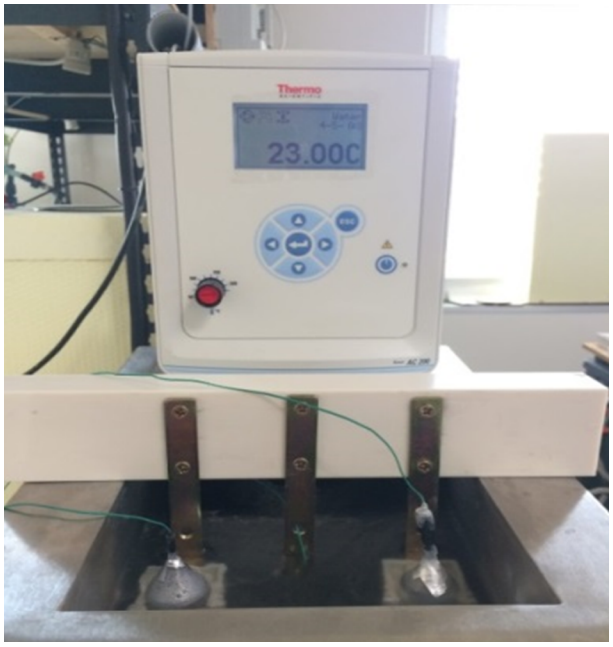

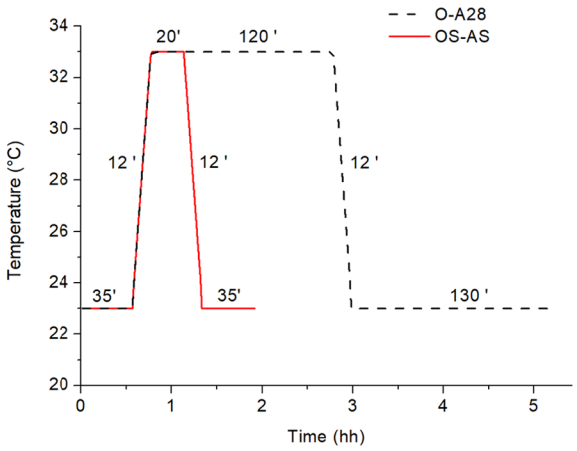

Step	O-A28		OS-AS	
	T(°C)	Time (min)	T(°C)	Time (min)
1	23	35	23	35
2	23-33	12	23-33	12
3	33	120	33	20
4	33-23	12	33-23	12
5	23	130	35	35

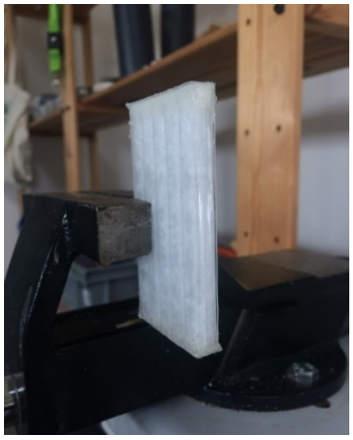

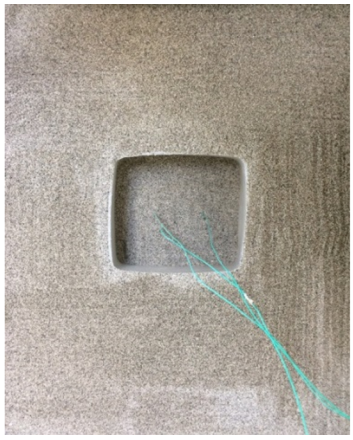

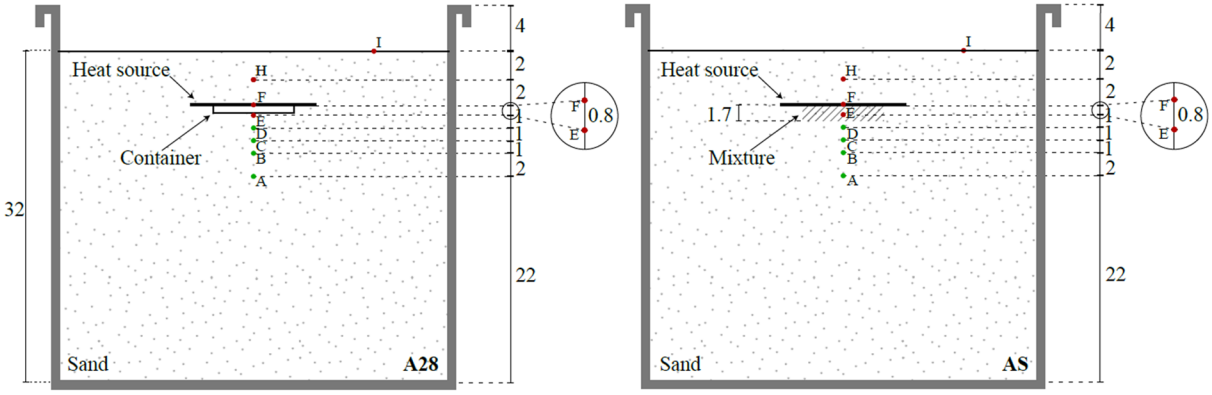

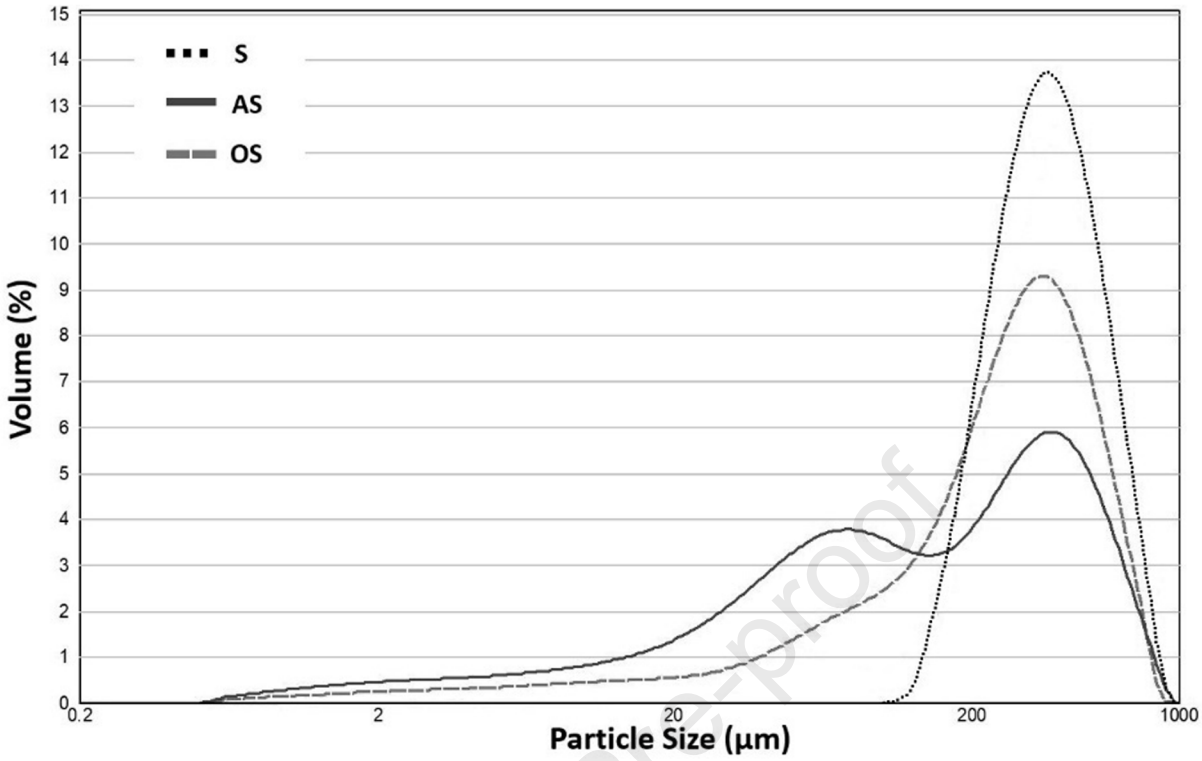

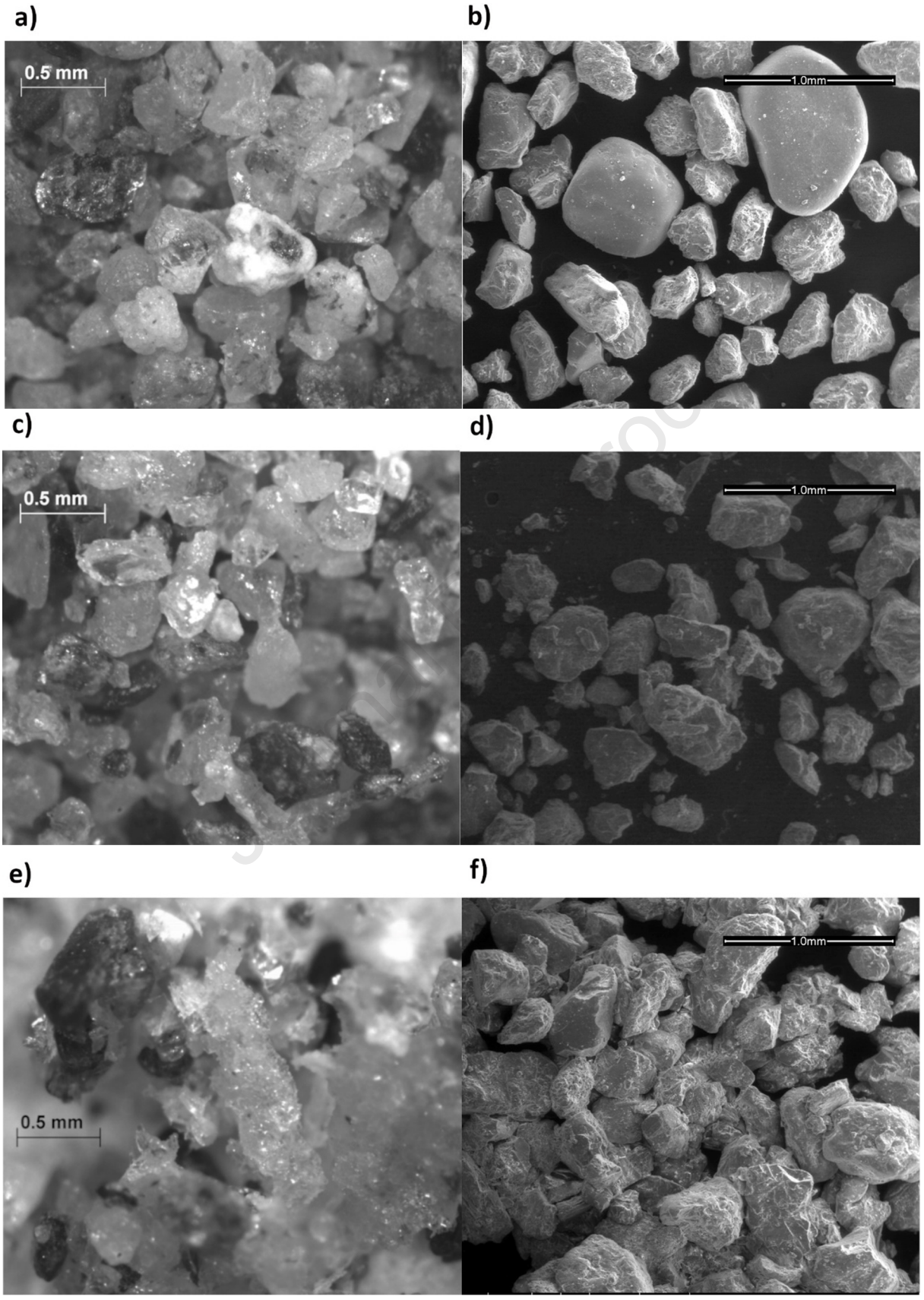
a)
0.5 mm
b)
1.0mm
c)
0.5 mm
d)
1.0mm
e)
0.5 mm
f)
1.0mm

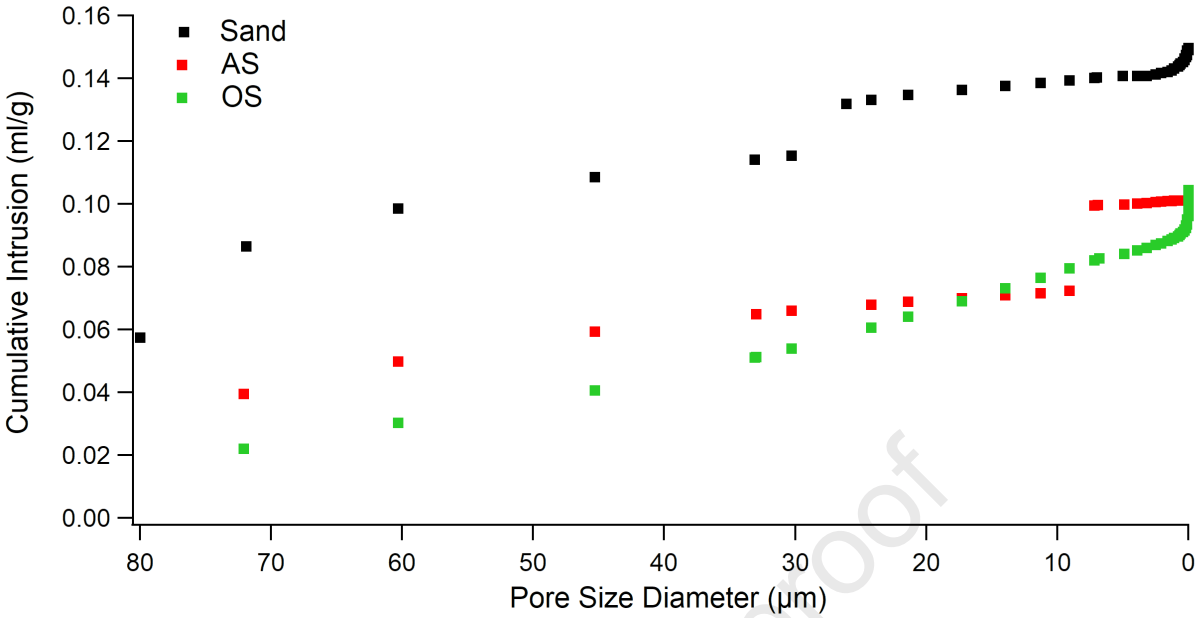

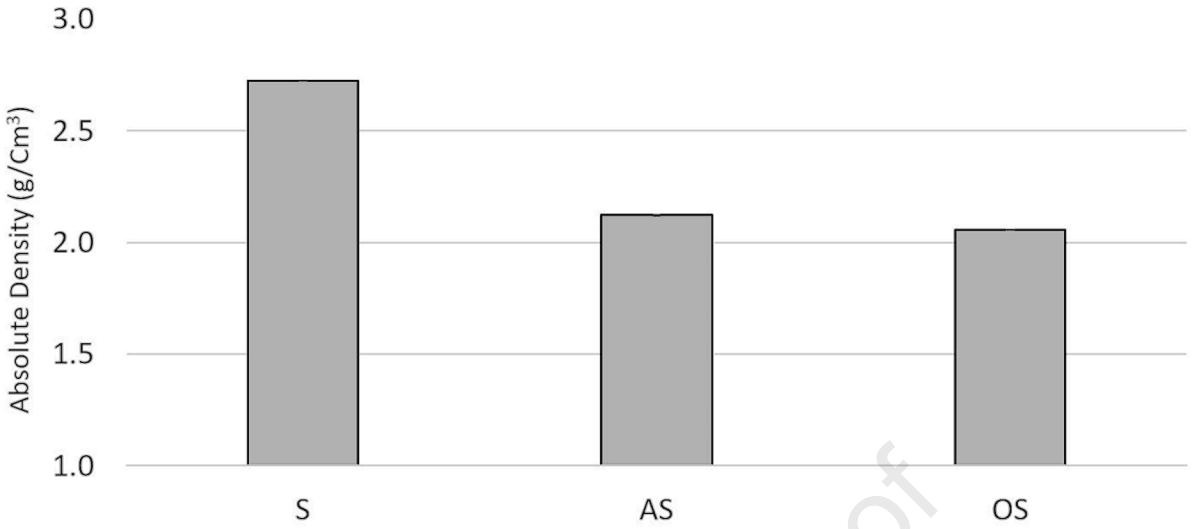

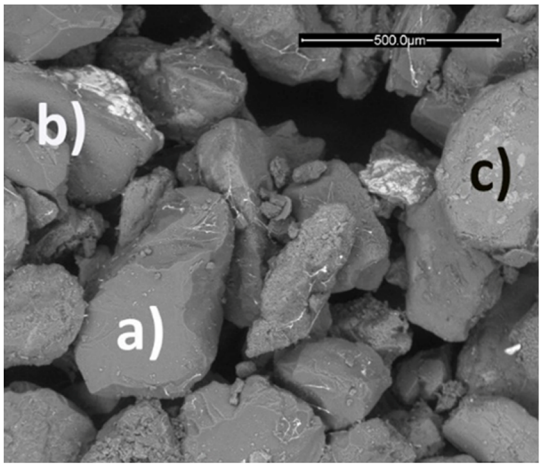

a)

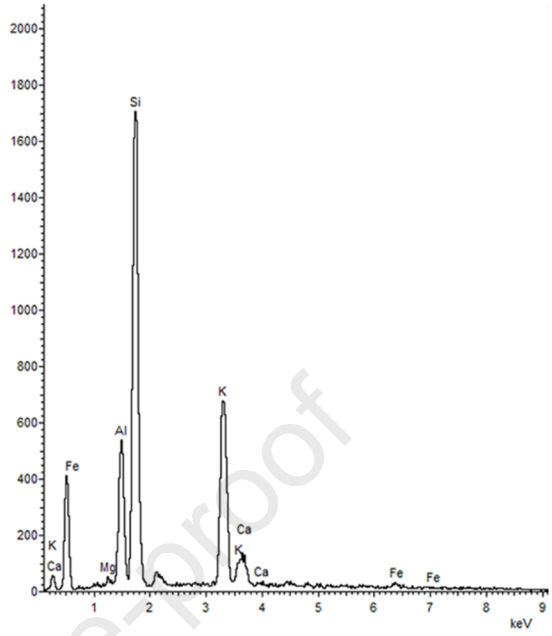

b)

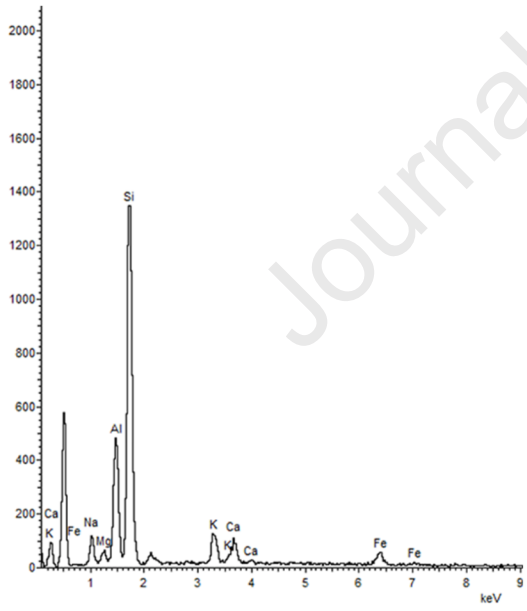

c)

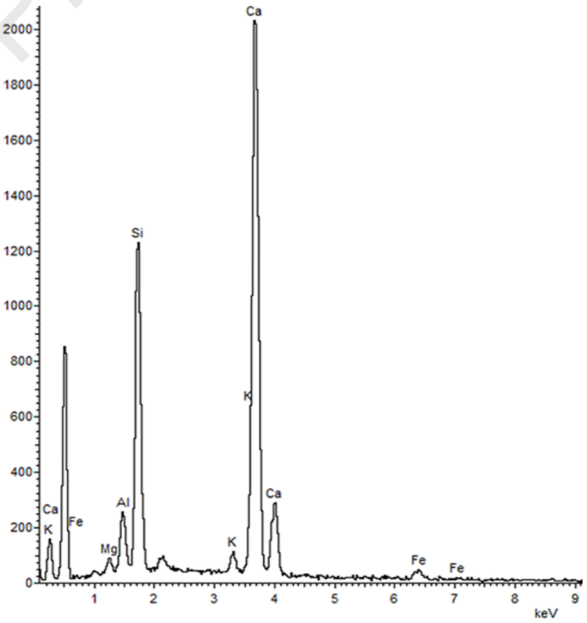

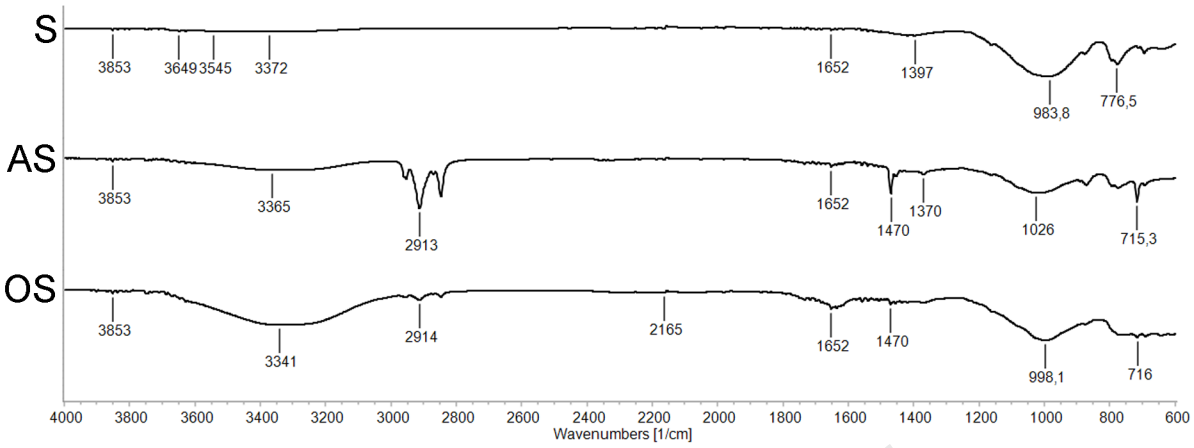

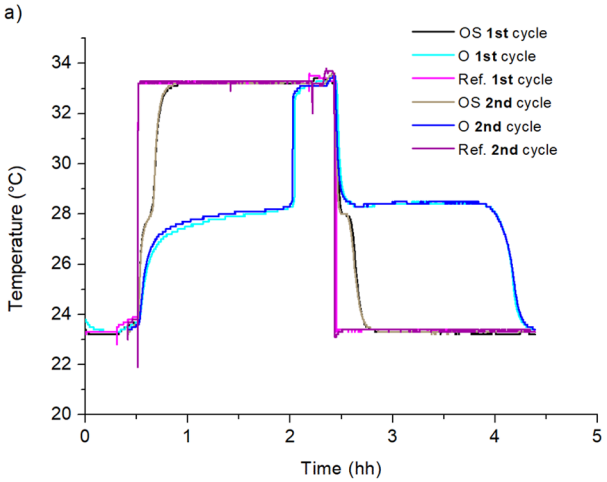

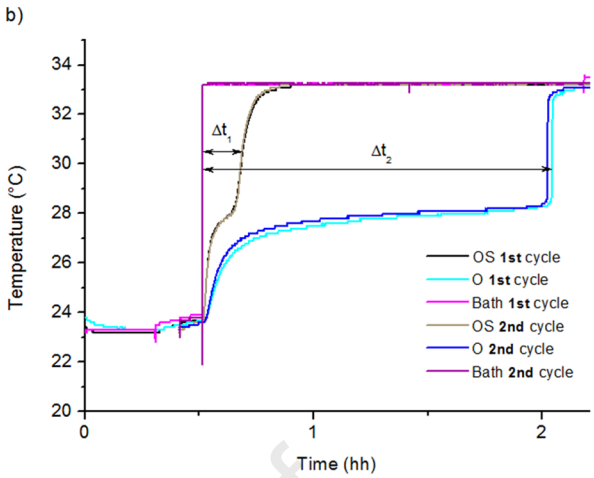

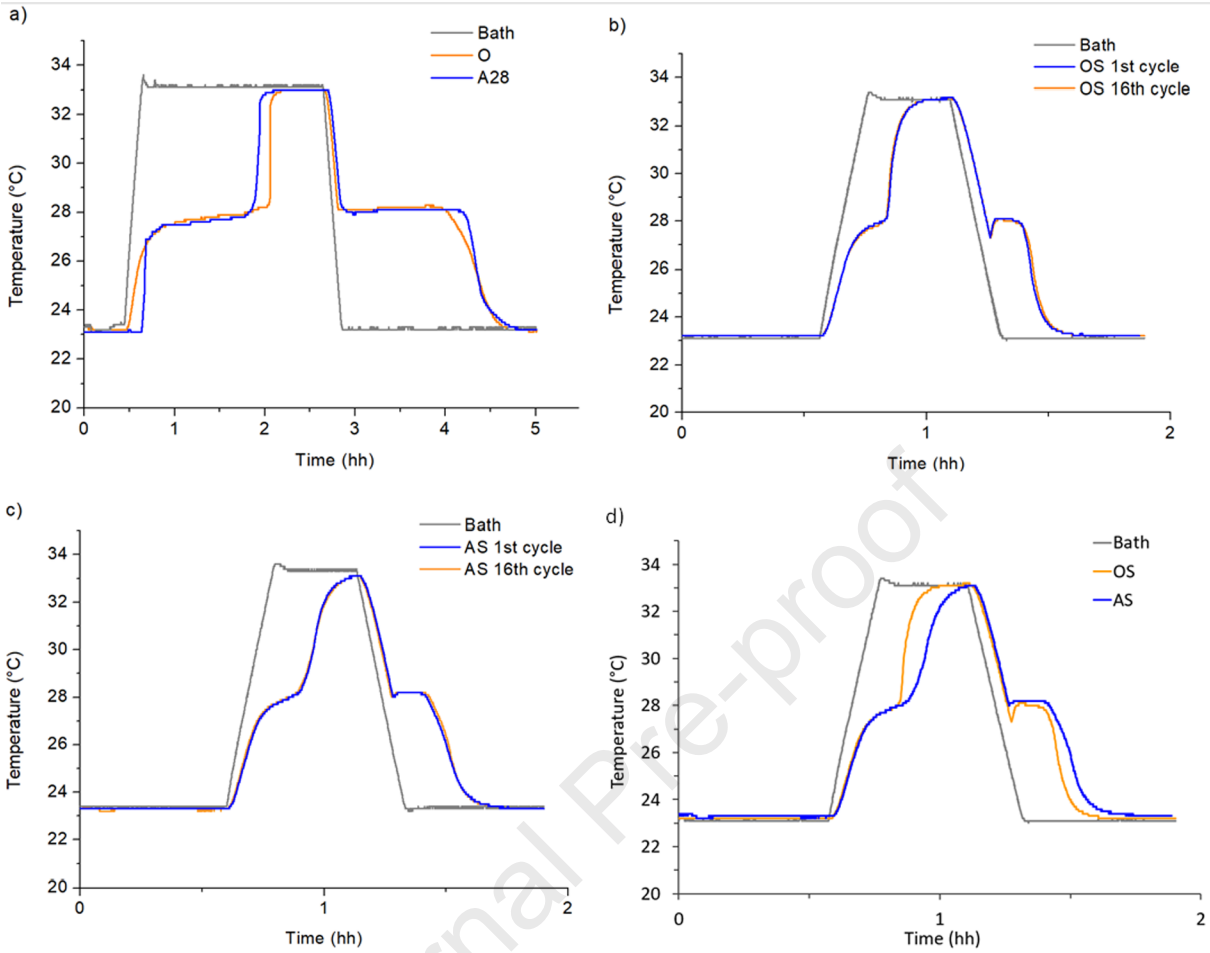

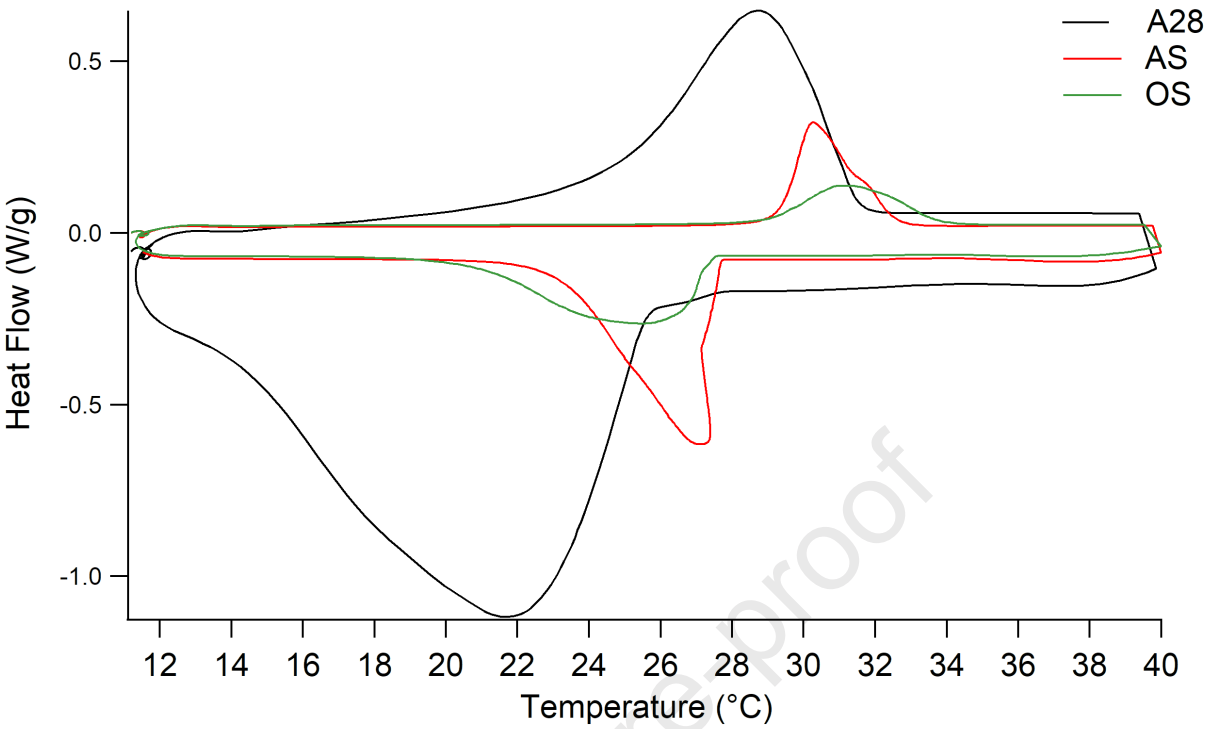

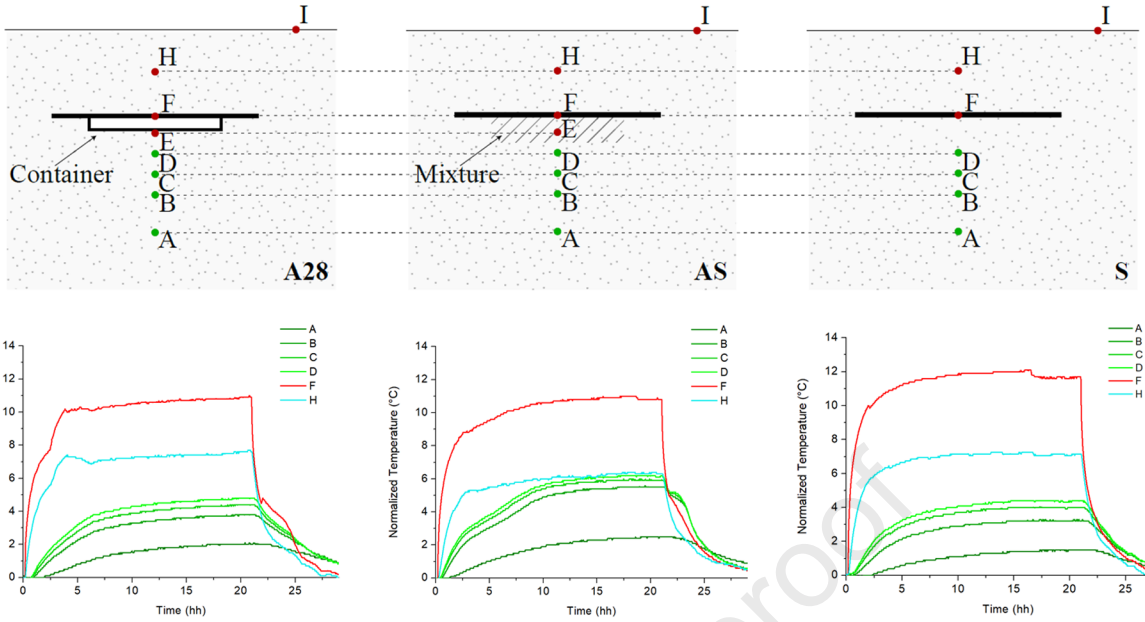

Highlights

- Paraffin-sand mixtures are PCMs suitable for LHTES coupled with shallow ground GHE.
- Paraffins' PCM thermal diffusivity is enhanced by sand addition (30:100).
- Thermal cycling over Paraffin-sand mixtures lead to sand grain size decreasing.
- Different chemical bonding occurs among pure and commercial paraffins.

Declaration of interests

X The authors declare that they have no known competing financial interests or personal relationships that could have appeared to influence the work reported in this paper.

☐The authors declare the following financial interests/personal relationships which may be considered as potential competing interests: